Targeting an anchored phosphatase-deacetylase unit restores renal ciliary homeostasis

Janani Gopalan

A dissertation

submitted in partial fulfillment of the

requirements for the degree of

Doctor of Philosophy

University of Washington

2020

Reading Committee: John D. Scott, Chair

Richard Gardner

Linda Wordeman

Program Authorized to Offer Degree: Pharmacology

University of Washington

ABSTRACT

Targeting an anchored phosphatase-deacetylase unit restores renal ciliary homeostasis

Janani Gopalan

Chair of the Supervisory Committee: John D. Scott

Department of Pharmacology

In the kidney, primary cilia projecting into the lumen of cells lining the inner medullary-collecting duct bend with urine flow to initiate intracellular signaling events. This mechano-sensory apparatus is defective in Polycystic Kidney Disease (PKD), inherited disorders that are characterized by the progressive formation of fluid-filled cysts in the kidney and end stage renal disease. Molecular defects include aberrant cAMP and calcium signaling, changes in apical actin, altered AQP2 trafficking and impaired formation of primary cilia.

My studies as a rotation student in the Scott lab led to an intriguing discovery, that loss of the A-Kinase Anchoring protein AKAP220, correlates with increased cilia formation and altered cilia morphology. Using CRISPR-Cas9 gene editing to modify AKAP220 such that it does not anchor protein-phosphatase 1 (PP1), I found that this phosphatase plays an important role in cilia formation through its interaction with histone deacetylase 6 (HDAC6), the depolymerizer of primary cilia. Loss of AKAP220-anchored PP1 inactivates HDAC6 and this led to hyper ciliation.

Further, proximity ligation assays showed that HDAC6 also interacts with AKAP220 and cycloheximide-chase degradation assays show that the anchoring protein dictates the stability of the deacetylase. Thus, drug-induced inactivation of HDAC6 restores control over ciliogenesis. Autosomal dominant polycystic kidney disease (ADPKD) is a common genetic disorder associated with abnormal cytoskeletal dynamics in the kidney collecting ducts and perturbed calcium and cAMP signaling in the ciliary compartment. Pharmacological blocking of local HDAC6 activity alters cilia development and reduces cystogenesis in kidney-on-chip and organoid models of ADPKD. These findings identify the AKAP220-PPI-HDAC6 pathway as a therapeutic target for ADPKD.

Table of Contents

Title....1
Abstract....3
Table of Contents....5
List of Figures and Tables....7
Glossary....8
Acknowledgements....9
Preface....10

Chapter 1 – Introduction to primary cilia

Introduction....11
Composition of the cilium....11
Histone deacetylase 6 (HDAC6)....13
Actin and primary cilia....14
Actin-associated proteins in ciliary maintenance....15

Chapter 2 – A-kinase anchoring protein (AKAP)-220

Introduction....17
AKAP220....17
PKA and GSK3....18
IQGAP1....18
PP1....19
Project aim....20

Chapter 3 – An anchored PP1-HDAC6 subcomplex regulates renal ciliary homeostasis

Abstract....21
Introduction....21
Results....23
Discussion....54
Materials and methods....58

Chapter 4 – AKAP220 regulates cell migration and adhesion

Abstract....63

Introduction....64

Cell migration....64

Cell-cell adhesion....66

AKAP-mediated signaling in cell migration and cell-cell adhesion....67

Results....69

Materials and methods....82

References....85

List of figures

Fig 1.1: Structure of the Primary cilium 12
Fig 1.2: Functional domains in HDAC6 13
Fig 1.3: Actin-associated proteins in ciliary maintenance 16
Fig 2.4: AKAP220 and its binding partners 19
Fig 3.1: Loss of AKAP220 enhances ciliogenesis 26
Fig 3.2: Deletion of AKAP150 has no effect on primary cilia development 28
Fig 3.3: AKAP220 influences tubulin deacetylation 32
Fig 3.4: Additional Proximity ligation (PLA) controls 34
Fig 3.5: Anchored protein phosphatase 1 is necessary for HDAC6 activity 37
Fig 3.6: Further characterization of AKAP220-ΔPP1 and tubacin action 39
Fig 3.7: Loss of AKAP220-PP1 subcomplex impacts actin reorganization 42
Fig 3.8: Cilia frequency and development are f-actin dependent 45
Fig 3.9: Characterizing the effect of actin-modulating drugs on AKAP220-ΔPP1 cilia 47
Fig 3.10: Loss of phosphatase anchoring promotes cilium elongation 50
Fig 3.11: Super resolution videos depicting flexibility of AKAP220KO cilia 52
Fig 3.12: Inactivating HDAC6 reduces renal cystogenesis 53
Fig 4.1: A migrating cell depicting the leading edge and localized proteins 65
Fig 4.2: Cell-cell adhesion contacts depicted between two cells 67
Fig 4.3: Cell proliferation assay 69
Fig 4.4: AKAP220 checks excessive cell spreading and enhanced cell-cell contact 71
Fig 4.5: Loss of AKAP220 results in elevated E-cadherin levels 72
Fig 4.6: Loss of AKAP220 results in elevated β-catenin levels 73
Fig 4.7: Loss of AKAP220 results in elevated β4 integrin levels 74
Fig 4.8: Cytochalasin-D treatment affects expression of CAMs 76
Fig 4.9: Jasplakinolide treatment affects expression of CAMs 78
Fig 4.10: Loss of AKAP220 enhances focal adhesion complexes 80
Fig 4.11: Proposed model of cell adhesion 81

Glossary

Abbreviation	Name
AKAP	A kinase anchoring protein
AQP2	aquaporin-2
AurA	aurora A
AVP	arginine vasopressin
cAMP	cyclic adenosine monophosphate
CytoD	cytochalasin D
ECM	extracellular matrix
FRAP	fluorescence recovery after photobleaching
GSK3β	glycogen synthase kinase 3β
HDAC6	histone deacetylase 6
HRP	horse radish peroxidase
IFT	intraflagellar transport
IMCD	inner medullary collecting duct
IQGAP	IQ domain containing GTPase activating protein
Jasp	Jasplakinolide
mIMCD3	mouse inner medullary collecting duct cell line
PBS	phosphate buffered saline
PCR	polymerase chain reaction
PFA	paraformaldehyde
PKA	protein kinase A
PKD	polycystic kidney disease
PLA	proximity ligation assay
PP1	protein phosphatase 1
Rac1	Ras-related C3 botulinum toxin substrate 1
RI	PKA regulatory subunit type I
RII	PKA regulatory subunit type II
SDS	sodium dodecyl sulfate
V2R	vasopressin type 2 receptor
µm	micrometer
µM	micromolar

Acknowledgements

I would like to sincerely thank my PhD advisor John for giving me the opportunity to work in his lab and conduct this work. Thank you, John, for your unwavering trust, support, and guidance during the most unprecedented situations. Special thanks to Rich Gardner for trusting me and giving me the opportunity to volunteer in his lab before I joined the program. Thank you, Rich. I am forever grateful for the chance you gave me. Thank you to my other committee members Beno Freedman, Linda Wordeman and Edith Wang for advice and constructive criticism over the years. A special thanks to the Beno for giving me the chance to learn new techniques and make some amazing friends in his lab. Thank you Ankita, Angela and Ramila for taking me into your fold and teaching me everything I know about kidney-on-a-chip.

Thank you to all Scott lab members past and present, with whom I have had the chance to interact. Mel's warm smile and hugs, Lorene's comforting words and Katherine's thoughtful insights have been a major part of my every day in the lab. Thanks, Donelson for all the discussions scientific and otherwise. Thanks, Mitch for always willing to listen to my project woes and brainstorm ideas. I will always remember you for lightening up dreary days with a dad joke or two. Thank you, Paula, and Stacey, my two best buds in lab for hours of conversations, coffee runs and lunch vent sessions. You two made my grad school more fun than I could have ever imagined. Thanks also to Jen, Leah, Laura, Kiana, Jerome, and Sophia. It has been a wonderful five years in the lab.

Thanks to my friends in the program-Jenny, you have taught me what resilience is and Harry, your wit has always had me in splits. Thanks to my partner Sriram for his unconditional love and unwavering support over the years, to my in-laws for always cheering me on and my daughter Ananya, for brightening my world endlessly. Lastly, my sincere thanks to my parents and sister. They have been my pillar of support and I am grateful to them for everything I am today.

Preface

Portions of the text and data from this dissertation are reprinted (adapted) from the following works under fair use and/or with permission under the terms of the CC-BY License:

Janani Gopalan, Ankita Roy, Mitch Omar, Nelly M. Cruz, Jerome Falcone, Katherine Forbush, Jonathan Himmelfarb, Benjamin S. Freedman, John D. Scott. 2020. Targeting an anchored phosphatase-deacetylase unit restores renal ciliary homeostasis. (under review)

CHAPTER 1: Primary cilia

Introduction

Primary cilia are microscopic, microtubule-based organelles, typically one per cell. They are ubiquitous in most vertebrate cell-types. Primary cilia are non-motile, and their assembly and disassembly are tightly coordinated with the cell cycle (Plotnikova et al., 2009). Defects in ciliary structure and/or function are associated with several debilitating disorders such as Bardet-Biedl syndrome, polycystic kidney disease and retinal disorders. These disorders are now collectively termed as ciliopathies (Badano et al., 2006). Although they were discovered much earlier, these organelles were originally considered to be vestigial with no function. The shift in perception of primary cilia was triggered in the 1990's by two important ideas- first, the ciliary hypothesis of polycystic kidney disease (PKD), that implicated dysfunctional primary cilia as basis for ciliopathies, and second, sonic-hedgehog signaling, a major neuro-developmental pathway was shown to require primary cilium for its signal transduction. Consequently, primary cilia are now considered to be "cellular antennae", that function as a signaling hub to dynamically concentrate and co-ordinate multiple inputs within their microscopic environment (Fliegauf et al., 2007).

Composition of the cilium

The centrosome serves as the main microtubule organizing center (MTOC) of the animal cell, as well as a key regulator of cell-cycle progression. The centrosome is comprised of mother and daughter centrioles. The mother centriole is also called the basal body, and this forms the base of the cilium (Lee et al., 2011). The stability of microtubules is influenced by the post-

translational modifications and other proteins associated with them. Stabilized acetylated microtubules form the axoneme or body of the primary cilium. Both primary and motile cilia contain axonemes of nine microtubule doublets. The axoneme microtubules (AxoMTs) bind motor proteins that transport cargo into and out of the cilium. This specialized transport system mediated by kinesin-2 (+ end) and dynein (- end) is called intra-flagellar transport (IFT) (Goetz and Anderson, 2010). Interestingly, the entire pool of ciliary proteins is transported from the cytoplasm since translation does not happen in this miniscule organelle. Although the primary cilium membrane is a continuation of the plasma membrane, the composition of proteins is distinct between the two (Long and Huang, 2020). The ciliary membrane is rich in phospho-inositides and transmembrane receptors involved in sensing and biochemical signaling. Over the last decade, a lot of work has focused on the composition of primary cilia, but the signaling mechanisms involved in ciliary homeostasis remain poorly understood.

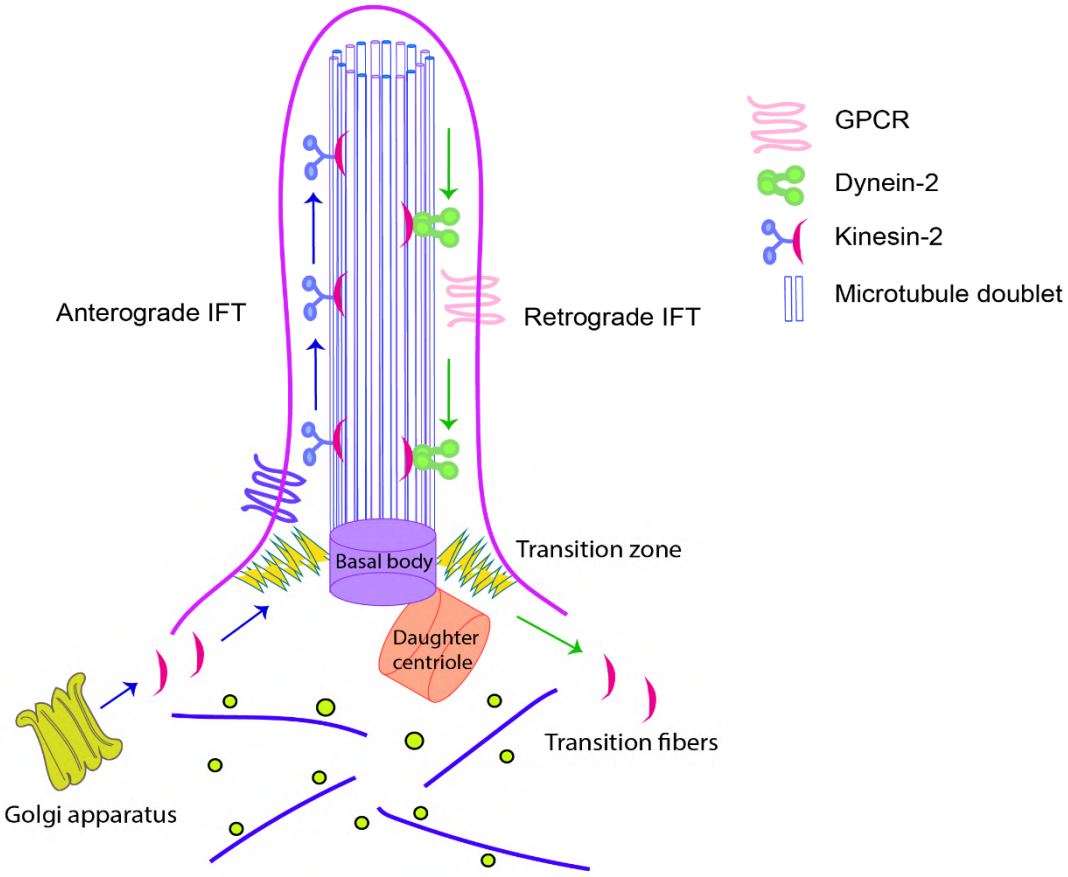

Fig 1: Structure of the Primary cilium

Ciliogenesis is a complex process dependent on the engagement of several signaling pathways and a variety regulating proteins. It is thought to begin one of two ways- the intracellular route where the basal body associates with a ciliary vesicle before tubulin and other proteins localize to the cilium, or the extracellular route where the basal body docks to a region of the apical membrane and then starts to assemble primary cilia (Goetz and Anderson, 2010). The mitotic kinase Aurora A (AurA) is the primary driver of cilia disassembly through activation of histone deacetylase 6 (HDAC6). This deacetylase and its interaction with the A kinase Anchoring protein AKAP220 and the type 1 phosphoprotein phosphatase PP1 are the primary focus of my project.

Histone deacetylase 6 (HDAC6)

HDAC6 has emerged as the major driver of cilia disassembly. This deacetylase localizes to the cytoplasm, centrosome and basal body and performs a variety of functions. Apart from tubulin, HDAC6 deacetylates cortactin, an actin binding protein and Hsp90 (Hubbert et al., 2002). HDAC6 is the only deacetylase that has a complete duplication of the class I/II HDAC homology domain (DD1 & 2). A nuclear export sequence (NES) is found in human and mouse HDAC6. An additional SE14 domain (present only in humans) serves to anchor HDAC6 to the cytoplasmic compartment. In the C-terminus, a zinc finger UBF confers ubiquitin-binding, DD1 and 2 are the deacetylase domains (Boyault et al., 2007) .

NES	**Nuclear exclusion**
DD1 and DD2	**Catalytic activity**
SE14	**Cytoplasmic anchoring**
ZnF-UBP	**Ubiquitin binding**

Fig 2: Functional domains in HDAC6

Deacetylase-dependent function: HDAC6 catalyzes the removal of acetyl groups from its substrates. It turns out that HDAC6 mediated deacetylation of tubulin and cortactin is necessary for cilia disassembly. But not all functions of HDAC6 require tubulin acetylation (TDAC) activity.

Ubiquitin-dependent function: HDAC6 is essential in mounting a cellular response to cytotoxic aggregates. A finely tuned equilibrium exists wherein excess HDAC6 delays the clearing of poly-ubiquitinated proteins due to its high-affinity binding to ubiquitin (Hubbert et al., 2002).

Actin and primary cilia

HDAC6 participates in actin polymerization and microtubule dynamics through its interaction with cortactin and formin homology domain proteins mDia1 and mDia2 (de Diego et al., 2014). Although actin and septin do not form the core of the axonemea, they localize to the base of the cilium to coordinate the assembly and disassembly of these microscopic organelles by. Actin polymerization to integral to several steps in ciliogenesis. Primary cilia form during the G0/G1 when basal body docks at the apical membrane. Cortical actin clearing commences and an axoneme is created. The basal body is connected to the surrounding actin cytoskeleton by focal adhesion complexes.

Actin mediates transport of ciliary membrane, IFT components and other cargo to the basal body via myosin II and myosin Va motor proteins. An appropriate balance of actin polymerization and depolymerization is necessary for maintenance of axoneme stability and length, yet the role of the actin-dependent process is poorly understood (Biologists, 2007). This is a bi-directional process where poor actin polymerization promotes cilia formation and enhanced actin polymerization attenuated ciliogenesis. One popular theory is the ciliary necklace hypothesis (Drummond et al., 2018). This model suggests that actin functions as a trafficking checkpoint for protein movement into the cilium. Loss of actin in this region could lead to unchecked protein movement and persistent primary cilia. Alternatively, another theory suggests that actin serves as a mechanical force to restrict cilia length. Relaxing the actin barrier surrounding the basal body could potentially provide more slack to the growing axoneme (Copeland et al., 2018). Several groups have performed pharmacological experiments to artificially polymerize or depolymerize actin using Jasplakinolide and Cyochalasin D respectively and found that loss of stabilized actin fibers increases cilia persistence and length.

Actin-associated proteins in ciliary maintenance

Cortactin is a classic example of an actin-binding protein that also regulates ciliogenesis. Cortactin recruits Arp2/3 to promote f-actin polymerization (Schnoor et al., 2018). Src-phosphorylation and HDAC6-mediated deacetylation of cortactin activate this protein to promote actin polymerization and therefore cause cilia disassembly. Conversely, missing in metastasis (MIM) promotes ciliogenesis by preventing Src phosphorylation of cortactin.

The Hippo signaling pathway controls organ size by regulating cell proliferation and apoptosis. Mouse mutants in Hippo pathway components display remarkable phenotypes of organ overgrowth, enhanced stem cell content and reduced cellular differentiation. YAP/TAZ are well known for being the effectors of the Hippo signaling cascade (Piccolo et al., 2014). Yes-associated protein 1 (YAP1) and WW-domain-containing transcription regulator 1 (WWTR1, referred to as TAZ) are transcriptional coactivators that induce expression of cell-proliferative and anti-apoptotic genes. Actin remodeling factors repress YAP/TAZ activity. F-actin filament bundling has been found to cause YAP inactivation, cell rounding, and ciliogenesis (Kim et al., 2015).

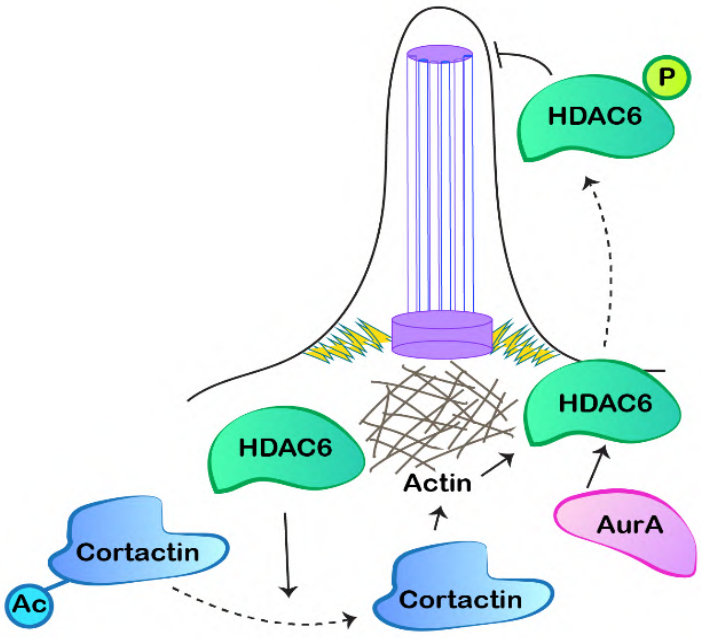

Fig 3: Actin-associated proteins in ciliary maintenance

Chapter 2: A-kinase anchoring protein (AKAP)-220

Introduction

Anchoring, adapter, and scaffolding proteins function to organize signaling elements such a kinases and phosphatases to modify the local phosphorylation/activity status of proteins in the vicinity (Scott and Pawson, 2009). A-kinase anchoring proteins (AKAPs) are scaffolding proteins that spatially constrain kinases, protein phosphatases and GTPase effector proteins within subcellular compartments (Bucko and Scott, 2021; Langeberg and Scott, 2015; Smith et al., 2017, 2018; Taskén and Aandahl, 2004; Whiting et al., 2015). A few anchoring proteins have been reported to reside in cilia (Choi et al., 2011; Jo et al., 2001; May et al., 2020; Stefan et al., 2007). Ciliary AKAPs have been postulated to position protein kinase A (PKA) as a negative regulator of hedgehog signaling (Breslow et al., 2018; Mukhopadhyay et al., 2013; Somatilaka et al., 2020). Furthermore, the primary cilium has been shown to be a cAMP signaling component, mediated by vasopressin receptor (V2R) in kidney epithelial cells.

AKAP220

This 220-KDa AKAP is encoded by the AKAP11 gene. It is ubiquitously expressed in a variety of tissues and cell types and is conserved in mammals. AKAP220 was originally reported to localize PKA to peroxisomes (Lester et al., 1996). Subsequent studies show that this scaffolding proteins targets PKA, GSK3, the Rho GTPase effector IQGAP-1 and protein phosphatase 1 (PP1) to specific compartments of the cell (Logue et al., 2011; Schillace and Scott, 1999; Whiting et al., 2015). Signaling complexes anchored by AKAP220 are known to regulate cytoskeletal dynamics. Specifically, AKAP220 sequesters IQGAP1 and the GTPase Rac to the leading edge of the cell during migration. Consequently, siRNA silencing of AKAP220 significantly affects formation of membrane ruffles and impairs migration of cells (Logue et al., 2011). Additionally, AKAP220 is also known to interact with aquaporin 2, a water channel protein in kidney collecting ducts. The kinase-phosphatase unit maintained by AKAP220 controls vasopressin-independent aspects of aquaporin-2 water channel trafficking to the apical membranes of cells lining the kidney collecting ducts (Whiting et al., 2016).

PKA and GSK3

Simultaneous anchoring of both kinases and phosphatases is essential for bi-directional control of signaling events. Kinases phosphorylate and invariably activate nearby substrates while phosphatases dephosphorylate and inactivate the signal transduction event. However, there are exceptions to this rule. AKAP220 anchors two kinases- PKA and GSK3. cAMP levels influence activity of each kinase. GSK3 is active at rest. However, when cAMP is elevated, phosphorylation by PKA inactivates it (Frame et al., 2001). Therefore, availability of cAMP promotes PKA phosphorylation events while inhibiting GSK3 signaling pathways.

IQGAP1

An AKAP220-IQGAP1 sub-complex influences cortical actin polymerization and microtubule

dynamics. This complex localizes to the leading edge of a migrating cell and promotes stability of microtubules. Silencing of AKAP220 using siRNA leads to blunting of lamellipodia and poor microtubule stability. Clip associating protein (CLASP2) interacts with IQGAP1 at the leading edge of cells. CLASP2 binds the plus-end of microtubules. Loss of AKAP220 from the leading edge mis-localizes IQGAP1 as well as CLASP2 and this leads to poor microtubule stability and slower migration (Logue et al., 2011). Interestingly, GSK3 phosphorylation of CLASP2 prevents this protein from interacting with IQGAP1 and microtubules. Therefore, local inhibition of GSK3 promotes CLASP2-IQGAP1 interaction and therefore cell migration.

PP1

AKAP220 has also been known to localize the catalytic subunit of protein phosphatase 1. Two separate PP1c interacting motifs were found in AKAP220. The consensus Lys-Val-Gln-Phe targeting motif (1195-1198) binds PP1c but does not affect enzyme activity (Schillace and Scott, 1999). A secondary motif (1711-1901) was found to inhibit the phosphatase activity. Truncation mutants of PP1c and PP1/2A catalytic subunits were used to identify the mechanism by which AKAP220 inhibits the phosphatase. The manner was distinct from known PP1 inhibitors and toxins (Schillace et al., 2001). Further, addition of PKA regulatory subunit further inhibited PP1 suggesting that components of the AKAP220 signaling complexes affect the catalytic activity of other binding partners.

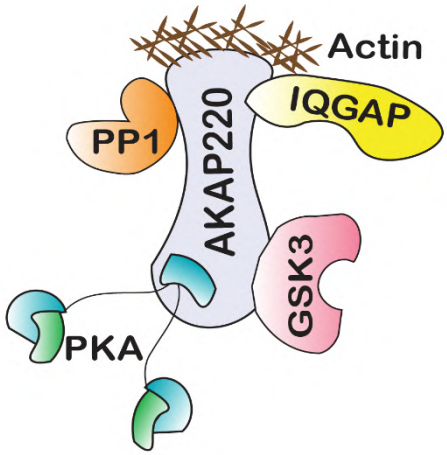

Fig 4: AKAP220 and its binding partners

Project aim

Protein phosphatase 1 has been purported to interact with histone deacetylase 6 (HDAC6) in the cytoplasm and localize to microtubules. PP1 binds the C-terminal domain of HDAC6 (Brush et al., 2004). Inhibitors of HDAC6 have been shown to prevent HDAC6-PP1 interaction by binding and inactivating HDAC6. Upon release from this complex, PP1 dephosphorylates Akt (Balliu et al., 2015). HDAC6 is the primary deacetylase of tubulin, cortactin and Hsp90 (Hubbert et al., 2002). As described in Chapter 1, HDAC6 activity drives primary cilia turnover.

The studies I began as a rotation student in the Scott lab led to a surprising discovery that loss of AKAP220 correlates with increased cilia formation and altered cilia morphology. Since then, I have used a combination of CRISPR/Cas9 gene-editing and super-resolution imaging of mouse

inner-medullary collecting duct IMCD3 cells to show that loss of AKAP220 correlates with a 7.2 ± 0.3 fold increase in primary cilia number and changes in cilia morphology. Surprisingly, this effect is recapitulated in gene-edited cells that express a mutated form of the anchoring protein that is unable to target protein phosphatase PP1. Thus, I envisaged a molecular mechanism whereby AKAP220 constrains the phosphatase PP1 to modulate cilia dynamics. Given AKAP220 localizes PP1 and this phosphatase forms a complex with HDAC6, we find that AKAP220 is essential for HDAC6 activity. Loss of AKAP220 or AKAP220-targeted PP1 inactivates HDAC6 and prevents cilia depolymerization. These findings are discussed in more detail in chapter 3.

CHAPTER 3: An anchored PP1-HDAC6 subcomplex regulates renal ciliary homeostasis.

Abstract

Pathophysiological defects in water homeostasis can lead to end-stage renal failure. Autosomal dominant polycystic kidney disease (ADPKD) is a common genetic disorder associated with abnormal cytoskeletal dynamics in the kidney collecting ducts and perturbed calcium and cAMP signaling in the ciliary compartment. We show that collecting ducts in mice lacking the A-Kinase anchoring protein AKAP220 exhibit enhanced development of primary cilia. Mechanistic studies reveal that AKAP220-associated protein phosphatase 1 (PP1) mediates this phenotype by promoting changes in the stability of histone deacetylase 6 (HDAC6) with concomitant defects in

actin dynamics. This proceeds through a previously unrecognized adaptor function for PP1 as all ciliogenesis and cytoskeletal phenotypes are recapitulated in mIMCD3 knock-in cells expressing a phosphatase-targeting defective AKAP220-ΔPP1 mutant. Pharmacological blocking of local HDAC6 activity alters cilia development and reduces cystogenesis in kidney-on-chip and organoid models of ADPKD. These findings identify the AKAP220-PPI-HDAC6 pathway as a therapeutic target for ADPKD.

Introduction

Kidneys recycle about 180 liters of fluid every day to partition nutrients and remove toxins from blood (Saborio et al., 2000). Water reabsorption from luminal fluid is triggered by the hormone arginine vasopressin via phosphorylation-dependent translocation of aquaporin-2 water pores to apical surface of kidney collecting ducts (Bankir et al., 2013; Noda et al., 2010; Yui et al., 2012). Not surprisingly, defects in renal water homeostasis have pathophysiological consequences. Approximately 35 million Americans suffer from chronic kidney diseases, characterized as a gradual loss of renal function (Hemmelgarn et al., 2006). Polycystic kidney diseases are disorders where the collecting ducts become enlarged with fluid filled cysts that reduce glomerular filtration rate (Wilson, 2004). Autosomal dominant polycystic kidney disease (ADPKD) with an estimated prevalence of 1 in 600 people, is a common genetic disorder associated with end-stage renal failure (Halvorson et al., 2010). Clinical evidence indicates that primary cilia function is altered in ADPKD (Ma et al., 2013, 2017). Hence this chronic renal disorder is classified as a ciliopathy (Badano et al., 2006; Fliegauf et al., 2007).

The primary cilium is a microtubule-based organelle protruding from the surface of most mammalian cells (Satir et al., 2010). In the kidney, primary cilia respond to fluctuations in fluid-

flow through collecting ducts (Dell, 2015). They convert mechanical stimuli into biochemical signals to elicit developmental and regulatory responses (Mukhopadhyay et al., 2013; Somatilaka et al., 2020). Disease causing mutations in the ciliary transmembrane proteins polycystin 1 (*PKD1*) and polycystin 2 (*PKD2*) underlie ADPKD (Hughes et al., 1995; Mochizuki et al., 1996). Both proteins are components of a receptor-channel complex that responds to local second messenger signals (Harris and Torres, 2014). Accordingly, a ciliary hypothesis has been formulated that implicates defective calcium and cAMP signaling in the ciliary compartment as a factor in disease progression (Ma et al., 2017; Winyard and Jenkins, 2011).

A-kinase anchoring proteins (AKAPs) spatially constrain second messenger regulated kinases, protein phosphatases and GTPase effector proteins within subcellular compartments (Bucko and Scott, 2021; Langeberg and Scott, 2015; Smith et al., 2017, 2018; Taskén and Aandahl, 2004; Whiting et al., 2015). Several AKAPs participate in renal signaling, yet only a few anchoring proteins reside in cilia (Choi et al., 2011; Jo et al., 2001; May et al., 2020; Stefan et al., 2007). Ciliary AKAPs are postulated to position protein kinase A (PKA) as a negative regulator of hedgehog signaling (Breslow et al., 2018; Mukhopadhyay et al., 2013; Somatilaka et al., 2020). AKAP220 is a multifunctional anchoring protein that sequesters PKA, GSK3, the Rho GTPase effector IQGAP-1 and protein phosphatase 1 (PP1) (Logue et al., 2011; Schillace and Scott, 1999; Whiting et al., 2015). Each AKAP220-binding partner is implicated in local signaling events that potentiate ADPKD. PKA and PP1 bi-directionally control signaling in the ciliary compartment, whereas reduced Rho GTPase activity contributes to expansion of renal cysts (Parnell et al., 2012; Ye et al., 2017).

Here we show that AKAP220$^{-/-}$ mice exhibit enhanced development of primary cilia. Mechanistic studies reveal that AKAP220 associated PP1 drives this phenotype by promoting changes in

actin dynamics and histone deacetylase 6 (HDAC6) stability. Pharmacological blocking of local HDAC6 activity alters cilia development and reduces cystogenesis in cellular models of ADPKD. These findings point towards the AKAP220-PPI-HDAC6 pathway as a therapeutic target for the treatment of ADPKD.

Results

Loss of AKAP220 promotes renal cilia assembly.

AKAP220 modulates cytoskeletal signaling events through its ability to recruit kinases, phosphatases and the small GTPase effector protein, IQGAP1 (Fig 1A; (Logue et al., 2011)). AKAP220$^{-/-}$ mice display mild defects in water homeostasis and altered aquaporin 2 (AQP2) trafficking that are linked to disruption of an apical actin barrier in the kidney collecting ducts (Fig 1B; (Whiting et al., 2016)). Further investigation in kidney sections from wildtype and AKAP220$^{-/-}$ mice led to the unexpected discovery that deletion of this anchoring protein correlated with increased numbers of primary cilia decorating each collecting duct (Fig 1C-H). The GTPase Arl13b (red) served as a ciliary marker, staining of AQP2 (green) marked kidney collecting ducts and DAPI (blue) highlighted nuclei (Fig 1C & D). Analysis of tissue sections collected from several animals are presented in Fig 1I, measuring a 3.5-fold increase in primary cilia in AKAP220$^{-/-}$, as compared to wildtype.

Independent validation of this observation was provided when CRISPR-Cas9 gene-editing was used to delete AKAP220 from mouse Inner Medullary Collecting Duct (mIMCD3) cells. Immunoblot analysis confirmed the loss of AKAP220 (Fig 1J, top panel, lane 2). GAPDH was used as loading control (Fig 1J, bottom panel). Immunofluorescent detection of primary cilia in clonal AKAP220KO cells measured a 10-fold increase in the percentage of ciliated cells in

comparison to wildtype mIMCD3 controls (Fig 1K-N). This phenotype was verified in another AKAP220 knockout clonal line (Fig 1M). Quantification is presented in Figure 1N. Rescue experiments allowed us to attribute this phenotype to the loss of AKAP220 (Fig 1O-T). AKAP220KO cells were transfected with a GFP-tagged AKAP220 construct (Fig 1O). Immunofluorescent detection of Arl13b (red) detected cilia and GFP-fluorescence confirmed rescue with the anchoring protein (Fig 1P &Q). GFP served as a control (Fig 1R &S). Quantification from three independent experiments confirmed that rescue with AKAP220 dramatically reduced the number of ciliated cells as compared to rescue with GFP (Fig 1T).

Renal spheroids recapitulate features of ductal architecture for disease modelling ((Giles et al., 2014); Fig 1U). We cultured mIMCD3 cells in Matrigel for 72 hours to form three-dimensional spheroids (Fig1 V & W). Immunofluorescent detection of the ciliary marker acetyl-tubulin (green) confirmed that loss of AKAP220 correlated with persistence of primary cilia in mIMCD3 KO spheroids (Fig1V-X). Detection of DAPI (blue) marked nuclei. Thus, local signaling mechanisms that proceed through AKAP220 impact ciliary development in cellular, three-dimensional spheroid and animal models of the renal microenvironment.

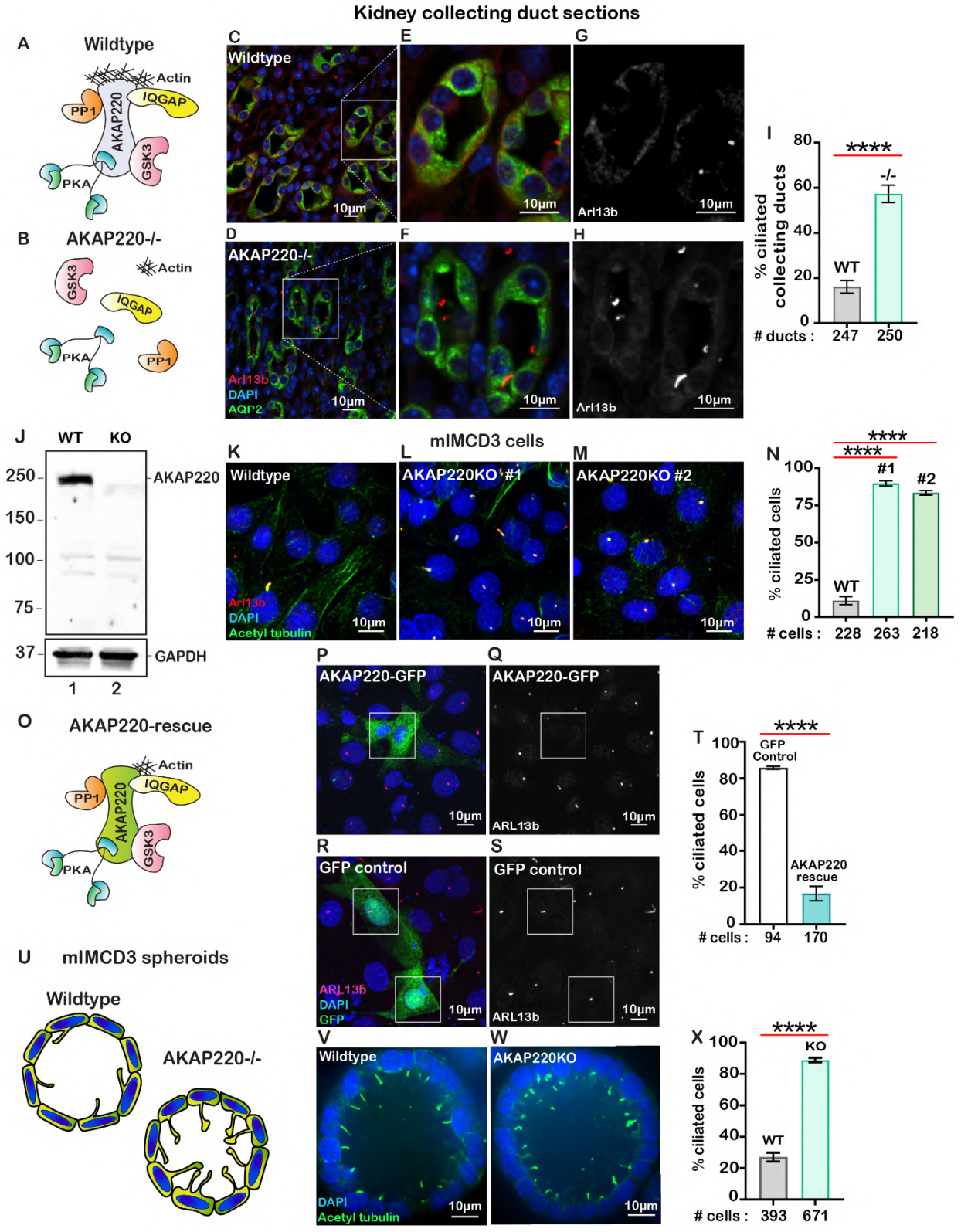
Kidney collecting duct sections
A
Wildtype
Actin
IQGAP
PP1
AKAP220
GSK3
PKA
B
AKAP220-/-
C
Wildtype
E
G
10μm
Arl13b
D
AKAP220-/-
F
H
Arl13b
DAPI
AQP2
I
% ciliated collecting ducts
****
-/-
WT
ducts : 247 250
J
WT KO
250
150
100
75
37
AKAP220
GAPDH
1 2
mIMCD3 cells
K
Wildtype
L
AKAP220KO #1
M
AKAP220KO #2
Acetyl tubulin
N
% ciliated cells
#1
#2
cells : 228 263 218
O
AKAP220-rescue
P
AKAP220-GFP
Q
ARL13b
R
GFP control
S
T
GFP Control
AKAP220 rescue
cells : 94 170
U
mIMCD3 spheroids
Wildtype
AKAP220-/-
V
W
AKAP220KO
X
KO
cells : 393 671

Figure 1: Loss of AKAP220 enhances ciliogenesis.

A) Schematic of AKAP220 interaction with selected binding partners. **B**) Disruption of this signaling complex upon removal of AKAP220. Protein kinase A (blue), Glycogen synthase kinase-3 (pink), Protein phosphatase 1 (orange) and IQGAP (yellow) are indicated. **C-H**) Immunofluorescent staining of kidney collecting ducts with Arl13b (red), Aquaporin-2 (green) and DAPI (blue) from **C**) wildtype and **D**) AKAP220$^{-/-}$ mice. **E & F**) Enlarged sections from wildtype and AKAP220$^{-/-}$ mice. **G & H**) Grey scale images of Arl13b. **I**) Quantification (% ciliated collecting ducts) in wildtype (grey bar) and AKAP220$^{-/-}$ (green bar). ****p<0.0001. Crispr-Cas9 gene editing of AKAP220 in mIMCD3 cells. **J**) Immunoblot detection of AKAP220 (top) and GAPDH loading control (bottom) from wildtype (lane 1) and AKAP220KO (lane 2) cell lysates. **K-M**) Immunofluorescent detection of primary cilia with acetyl tubulin (green), Arl13b (red) and DAPI (blue) in wildtype, and two independent clones of AKAP220KO mIMCD3 cells. **N**) Quantification (% ciliated cells) from wildtype (grey column), AKAP220KO#1 (green column) and AKAP220KO#2 (dark green column). ****p<0.0001, N=3. **O**) Schematic depicting reformation of the signaling complex upon rescue with AKAP220. Immunofluorescent detection of Arl13b (pink), GFP (green) and DAPI (blue) in **P**) pEGFP-AKAP220 or **R**) GFP-control transfected AKAP220KO mIMCD3 cells. Grey scale image of Arl13b in **Q**) control cells and **S**) AKAP220-rescued cells. **T**) Quantification (% ciliated cells) in pEGFP-AKAP220 (black bar) or GFP-control cells (teal bar). ****p<0.0001, N=3. **U**) Schematic of wildtype and AKAP220KO mIMCD3 spheroids. Immunofluorescent staining with acetyl tubulin (green) and DAPI (blue) in **V**) wildtype and **W**) AKAP220KO spheroids. **X**) Quantification (% ciliated cells) in wildtype (grey column) and AKAP220KO (green column) spheroids. ****p<0.0001, N=3. All error bars are s.e.m. *P* values were calculated by unpaired two-tailed Student's t-test. Scale bars (10μm). Number of cells analyzed indicated below each column.

Since another anchoring protein AKAP150 has been detected in primary cilia, it was important to establish if this AKAP also contributed to primary cilia development (Choi et al., 2011). Gene-editing was used to generate mIMCD3 cells lacking AKAP150. Double knockout cells lacking AKAP150 and AKAP220 were also produced. Immunofluorescent detection of ARl13b (green) and acetyl-tubulin (red) as ciliary markers revealed that the loss of AKAP150 alone had no effect on cilia development (Supp Fig 1A & B). Yet, a pronounced increase in the ciliated population was observed in AKAP220/150 double knockout cells (Supp Fig 1C & D). These additional studies indicate that AKAP150 signaling does not support renal ciliogenesis.

Figure 1 supplement

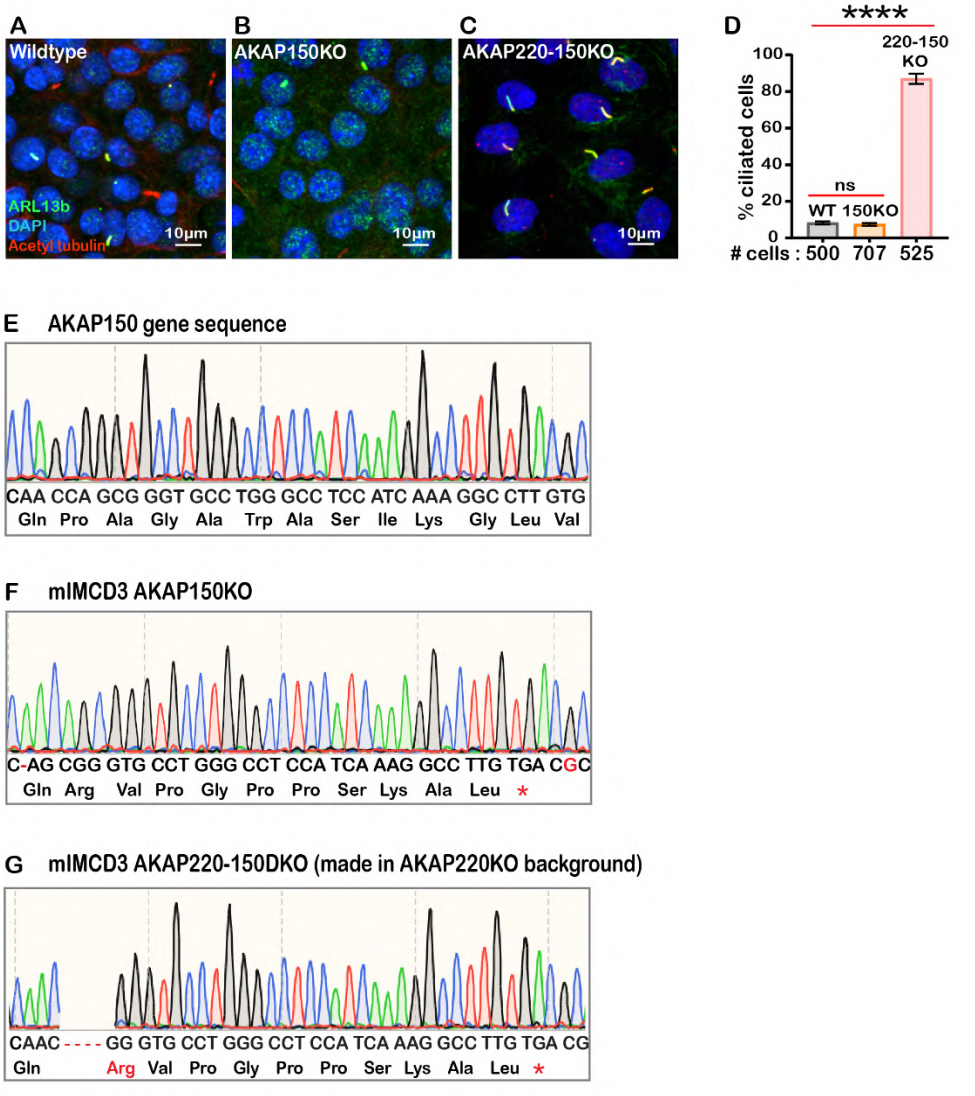

Supplemental figure 1: Deletion of AKAP150 has no effect on primary cilia development.

Crispr-Cas 9 gene editing was used to delete the murine anchoring protein AKAP150 in mIMCD3 cells. Double knockout cells were also produced lacking AKAP220 and AKAP150. Immunofluorescent staining with ciliary markers Arl13b (green) and acetyl tubulin (red) in **A**) wildtype, **B**) AKAP150KO and **C**) AKAP220-150KO mIMCD3 cells. DAPI serves as a nuclear marker. **D**) Quantification (% ciliated cells) in wildtype (grey column), AKAP150KO (orange column) and AKAP220-150KO (coral column). Number of cells analyzed are indicated below each bar. ****p<0.0001, ns=non-significant, N=3. Error bars are s.e.m. *P* values were calculated by unpaired two-tailed Student's t-test. Scale bars (10μm). CRISPR-Cas9 gene editing was used to disrupt the AKAP150 gene to generate AKAP150 and AKAP220-150 double knockout mIMCD3 cells. Sequencing analysis data shows **E**) intact AKAP150 in wildtype AKAP150, and deletions of AKAP150 in **F**) AKAP150KO cells and **G**) AKAP220-150 double knockout cells made in AKAP220KO background.

AKAP220 contributes to histone deacetylase 6 stability.

Primary cilia formation requires tubulin heterodimers that are stabilized by acetylation on lysine 40 (Portran et al., 2017). This prompted us to consider whether acetylated tubulin was abundant in cells lacking AKAP220. Experiments were conducted in two phases. First, immunofluorescent detection of acetylated alpha tubulin confirmed that this modified form was prevalent in AKAP220KO cells (Fig 2A & B). Second, immunoblot analysis showed that acetyl tubulin was more prominent in AKAP220KO cell lysates as compared to wildtype (Fig 2C, top panel). Alpha tubulin was consistent in both cell lines (Fig 2C, mid panel). GAPDH was the loading control (Fig 2C, lower panel). Amalgamated data from four independent experiments are quantified in figure 2D.

Histone deacetylase 6 (HDAC6) catalyzes the de-acetylation of tubulin to promote depolymerization of primary cilia (Hubbert et al., 2002; Ran et al., 2015). Hence, we reasoned that the enhanced detection of acetylated tubulin in AKAP220KO cells may be a consequence of reduced HDAC6 activity. Five complementary methods tested this postulate. First, immunofluorescent detection of HDAC6 (cyan) confirmed its enhanced compartmentalization at the base of primary cilia in wildtype mIMCD3 cells (Fig 2E & F). Conversely, the subcellular distribution of HDAC6 was ameliorated in AKAP220KO mIMCD3 cells (Fig 2G & H). This is most apparent in the grey scale images representing HDAC6 alone (Fig 2F & H). DAPI served as a nuclear marker (Fig 2E & G). Second, immunoblot analysis of HDAC6 protein in mIMCD3 cell lysates detected reduced levels of the deacetylase in cells that lack AKAP220, as compared to wildtype controls (Fig 2I, top panel, lane 2). GAPDH served as a loading control (Fig 2I, bottom panel). Amalgamated data from five independent experiments indicated that deletion of AKAP220 correlated with a 50% reduction of total HDAC6 in mIMCD3 cells (Fig 2J). This argues that interface with AKAP220 serves to stabilize HDAC6.

Third, proximity ligation assay (PLA) detected AKAP220-HDAC6 complexes in situ. This approach amplifies protein-protein interactions that occur within a range of 40–60 nm (Whiting et al., 2015). PLA puncta indicative of AKAP220/HDAC6 complexes were readily detected in cells transfected with V5-tagged AKAP220 (Fig 2K). Grey scale image emphasizes the distribution of AKAP220.HDAC6 complexes (Fig 2L). In contrast, detection of PLA puncta was dramatically reduced in control experiments performed in untransfected cells or in the absence of HDAC6 or V5 antibodies (Fig 2M & N, Supp Fig 2). GFP was used as a transfection marker. Quantification from three independent experiments is presented (Fig 2O).

Fourth, we performed cycloheximide-chase experiments. Cells lysates were prepared at selected time points (0-4 hours; Fig 2P). Immunoblot detection of HDAC6 (top panel) and acetylated tubulin (mid panel) monitored the stability and activity of the de-acetylase over time. GAPDH served as a loading control (bottom panel). In wildtype mIMCD3 cells, HDAC6 protein was relatively constant and acetylated tubulin levels were low (Fig 2P, lanes 1-3). Conversely, upon loss of the anchoring protein, HDAC6 levels were markedly reduced over time and acetylated tubulin levels were elevated (Fig 2P, lanes 4-6). Densitometric analysis of HDAC6 levels in wildtype (grey) and AKAP220KO (green) from three independent experiments are presented (Fig 2Q). Finally, overexpression of murine HDAC6 (cyan) abrogated primary cilia formation in AKAP220KO cells (Fig 2R & S). In contrast, expression of a catalytically inactive HDAC6 mutant (H216A, H611A) had no effect on cilia formation in the AKAP220 null background (Fig 2T & U). Amalgamated data from three experiments are presented (Fig 2V). Collectively, these studies implicate HDAC6 activity in AKAP220-mediated control of primary cilia development. Mechanistically, dephosphorylation of HDAC6 favors its degradation (Ran et al., 2020). Protein phosphatase 1(PP1) is a well-characterized binding partner of AKAP220 that also interacts with this deacetylase (Brush et al., 2004). Therefore, we reasoned that PP1 may serve as an adaptor protein that bridges HDAC6 to AKAP220 at the ciliary compartment (Fig 2W).

Figure 2

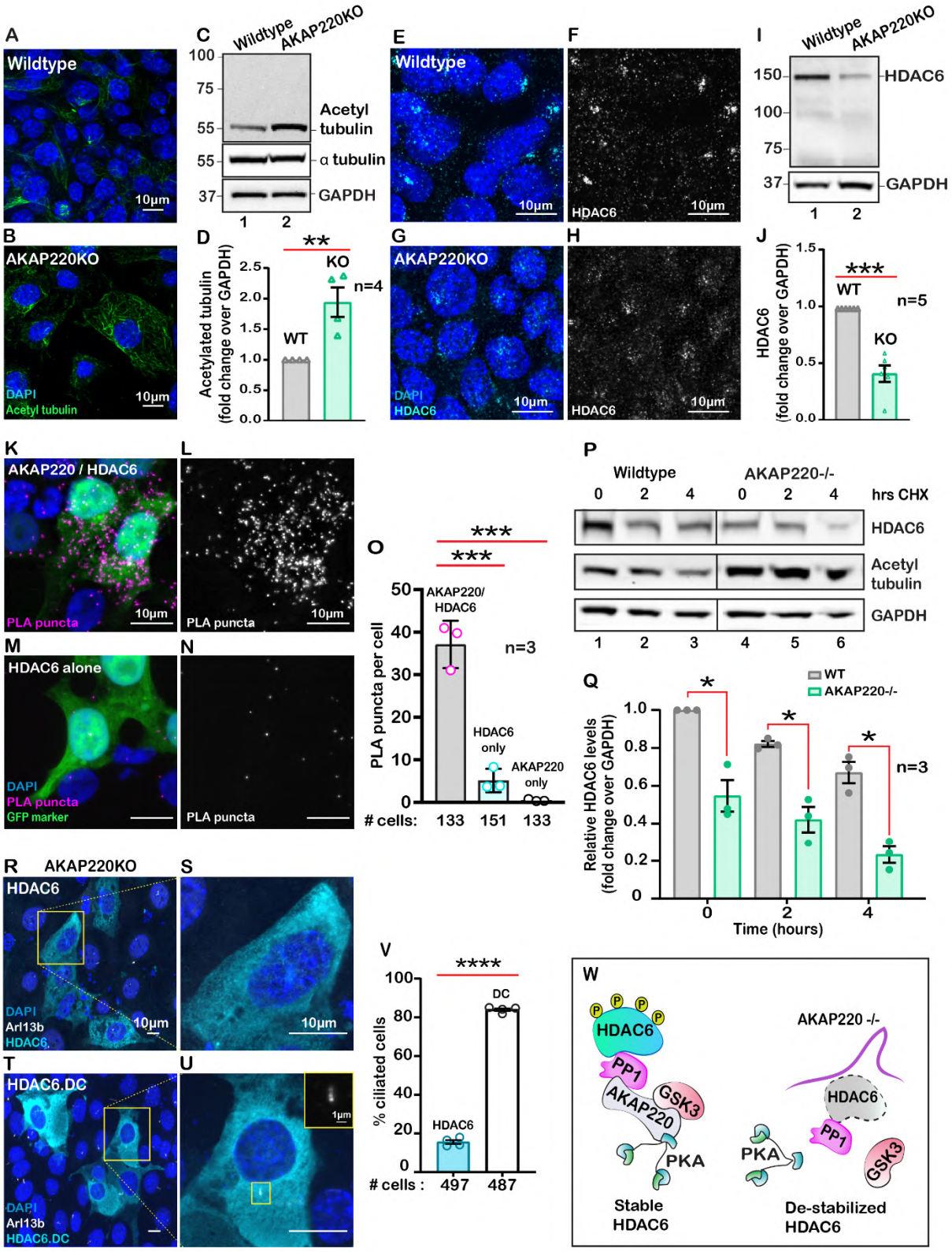
A
Wildtype
10μm
B
AKAP220KO
DAPI
Acetyl tubulin
10μm
C
Wildtype
AKAP220KO
100
75
55
55
37
Acetyl tubulin
α tubulin
GAPDH
1
2
D
**
KO
n=4
WT
Acetylated tubulin (fold change over GAPDH)
2.5
2.0
1.5
1.0
0.5
0.0
E
Wildtype
10μm
F
HDAC6
10μm
G
AKAP220KO
DAPI
HDAC6
10μm
H
HDAC6
10μm
I
Wildtype
AKAP220KO
150
100
75
37
HDAC6
GAPDH
1
2
J
***
WT
KO
n=5
HDAC6 (fold change over GAPDH)
1.5
1.0
0.5
0.0
K
AKAP220 / HDAC6
PLA puncta
10μm
L
PLA puncta
10μm
M
HDAC6 alone
DAPI
PLA puncta
GFP marker
N
PLA puncta
O
***
***
AKAP220/ HDAC6
n=3
HDAC6 only
AKAP220 only
PLA puncta per cell
50
40
30
20
10
0
cells:
133
151
133
P
Wildtype
AKAP220-/-
0
2
4
0
2
4
hrs CHX
HDAC6
Acetyl tubulin
GAPDH
1
2
3
4
5
6
Q
WT
AKAP220-/-
*
*
*
n=3
Relative HDAC6 levels (fold change over GAPDH)
1.0
0.8
0.6
0.4
0.2
0
0
2
4
Time (hours)
R
AKAP220KO
HDAC6
DAPI
Arl13b
HDAC6
10μm
S
10μm
T
HDAC6.DC
DAPI
Arl13b
HDAC6.DC
U
1μm
V
****
DC
HDAC6
% ciliated cells
100
80
60
40
20
0
cells :
497
487
W
HDAC6
P
PP1
AKAP220
GSK3
PKA
Stable HDAC6
AKAP220 -/-
HDAC6
PP1
PKA
GSK3
De-stabilized HDAC6

Figure 2: AKAP220 influences tubulin deacetylation.

Immunofluorescent detection of acetyl tubulin (green) and DAPI (blue) in **A**) wildtype and **B**) AKAP220KO mIMCD3 cells. **C**) Immunoblot detection of acetylated tubulin (top), alpha tubulin (mid) and GAPDH loading control (bottom), in wildtype (lane 1) and AKAP220KO (lane 2) cell lysates. **D**) Quantification by densitometry of acetylated tubulin in wildtype (grey column) and AKAP220KO (green column) lysates. **p<0.01, N=4. Immunofluorescent staining of HDAC6 (cyan) and DAPI (blue) in **E**) wildtype and **G**) AKAP220KO cells. Grey scale images of HDAC6 in **F**) wildtype and **H**) AKAP220KO cells. **I**) Immunoblot detection of HDAC6 (top) and GAPDH as loading control (bottom) in wildtype (lane 1) and AKAP220KO (lane 2) cell lysates. **J**) Quantification by densitometry of HDAC6 in wildtype (grey column) and AKAP220KO (green column) lysates. ***p<0.001, N=5. **K**) Proximity ligation (PLA) detection of V5-AKAP220/HDAC6 subcomplexes (pink), DAPI (blue) in cells expressing GFP (green) as a transfection marker. **L**) Grey scale image highlights V5-AKAP220/HDAC6 PLA puncta. **M** & **N**) Control PLA experiments in cells treated with anti-HDAC6 antibody alone. **O**) Amalgamated data (PLA puncta/cell) from three independent experiments is presented. Cycloheximide pulse-chase assay investigated HDAC6 stability. **P**) Immunoblot of HDAC6 (top), acetylated tubulin (mid) and loading control GAPDH (bottom) from wildtype (lanes 1-3) and AKAP220KO (lanes 4-6) from mIMCD3 cells treated with cycloheximide. Data collected over a time course (0-4 h). **Q**) Quantification of amalgamated data by densitometry (N=3). HDAC6 levels in wildtype (grey) and AKAP220KO (green) are indicated. Levels of protein are normalized to wildtype control (no treatment, 0hr). **R-V**) AKAP220KO mIMCD3 cells were transfected with **R**) flag-HDAC6 or **T**) catalytically inactive mutant HDAC6.DC. Immunofluorescent detection of HDAC6 (cyan), Arl13b (white) and DAPI (blue). Enlarged sections depict **S**) loss of primary cilium upon overexpression of active HDAC6 and **U)** intact cilium upon overexpression of inactive mutant HDAC6.DC. **V**) Quantification (% ciliated cells) in AKAP220KO cells transfected with flag-HDAC6 (black

column) and HDAC6.DC (cyan column). ****p<0.0001, N=3. **W**) Schematic of how recruitment to the AKAP220-signaling complex stabilizes HDAC6 through local phosphorylation. All error bars are s.e.m. *P* values were calculated by unpaired two-tailed Student's t-test. Scale bars (10μm). Number of cells analyzed indicated below each column.

Figure 2 supplement

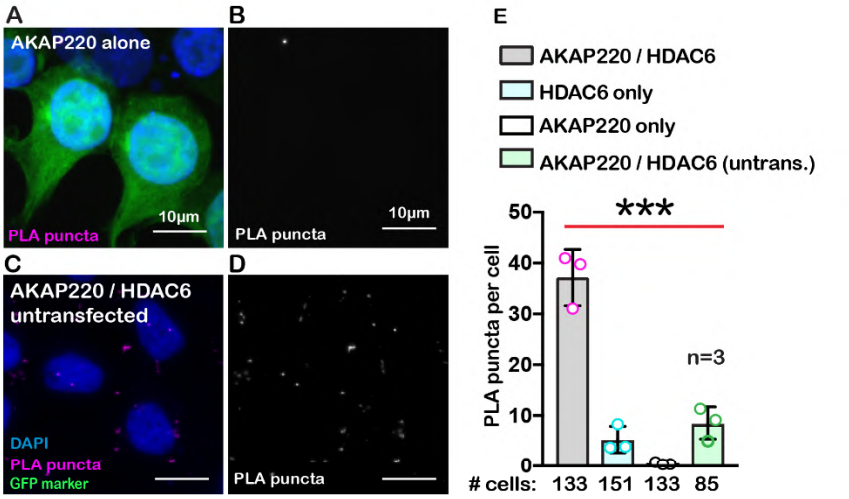

Supplemental figure 2: Additional Proximity ligation (PLA) controls

Proximity ligation (PLA) detection of V5-AKAP220/HDAC6 subcomplexes (pink), DAPI (blue) in cells expressing GFP (green) as a transfection marker in mIMCD3 cells **A**) transfected with V5-AKAP220 only and **C**) AKAP220/HDAC6 untransfected. **B**) and **D**) Grey scale image highlights V5-AKAP220/HDAC6 PLA puncta. **E**) Amalgamated data (PLA puncta/cell) from three independent experiments is presented.

AKAP220-anchored protein phosphatase 1 alters primary cilia turnover.

Protein phosphatase 1 interacts with AKAP220 primarily through its KVQF motif (Schillace and Scott, 1999), and has recently been implicated in trafficking of polycystin-1 to cilia (Luo et al., 2019). We used CRISPR-Cas9 gene editing to generate a knock-in cell line where the phosphatase-targeting motif was replaced by a TATA sequence (Fig 3A & 3B). Immunoblot analysis confirms expression of AKAP220-ΔPP1 as compared to knockout control (Fig 3C, top panel, lane 2). GAPDH was a loading control (Fig 3C, bottom panel). Co-immunoprecipitation assays confirmed that AKAP220-ΔPP1 is unable to anchor PP1 (Supp Fig 3C). To our surprise, characterization by immunofluorescence revealed that loss of a mere four-residue motif that enables PP1-anchoring to AKAP220 correlated with dramatically increased cilia numbers (Fig 3D & E). Arl13b(red) and acetyl tubulin (green) were used as ciliary markers and nuclei were detected by DAPI (blue). This striking phenotype is clearly portrayed in the gray scale images of Arl13b (Fig 3F & G). Additionally, three-dimensional surface plots show that primary cilia morphology is altered in the AKAP220- ΔPP1 cells, as compared to wildtype controls (Fig 3H & I). Results from at least three independent experiments are quantified (Fig 3N). Parallel analyses established that acetyl-tubulin was elevated in AKAP220-ΔPP1 (Fig 3J & L). This is highlighted in insets and 3D surface plots of acetylated tubulin (Fig 3K & M). Collectively, these results indicate that loss of PP1-anchoring to AKAP220 is necessary and sufficient to enhance ciliary development.

We reasoned that PP1 may serve as an adaptor protein that incorporates histone deacetylase 6 into AKAP220 signaling complexes. The HDAC6-selective inhibitor tubacin was used as a tool to evaluate the contribution of this enzyme activity in our mIMCD3 cell lines ((Haggarty et al., 2003); Fig 3O). Experiments were conducted in two phases. First, acetylated tubulin levels were monitored in each cell type by immunoblot (Fig 3P, lanes 1-3). Parallel samples were treated

with tubacin to inactivate HDAC6 (Fig 3P, lanes 4-6). GAPDH was a loading control (Fig 3P, bottom panel). Acetylated tubulin was elevated in AKAP220KO and to a lesser extent in AKAP220-ΔPP1 cells. Second, a fluorometric assay monitored enzyme activity in each cell type (Fig 3Q). As expected, HDAC6 activity was reduced in AKAP220KO and AKAP220-ΔPP1, as compared to the wildtype mIMCD3 cells. Amalgamated data from four experiments are presented (Fig 3Q). These findings suggest that the loss of HDAC6 activity and elevated acetylated tubulin correlate with persistence of primary cilia.

This led to a working hypothesis that AKAP220-targeted HDAC6 modulates primary cilia development. Therefore, tubacin was applied to test if blocking anchored-HDAC6 activity enhanced ciliary development. In wildtype cells, application of tubacin (2μM) increased the number of ciliated cells as assessed by immunofluorescent detection of Arl13b (red) and acetylated tubulin (green; Fig 3R & T). The grey scale image and quantification of three independent experiments reveal a 3.2-fold increase in percent ciliated cells upon pharmacologically targeting HDAC6 (Fig 3V & X). Co-staining with both cilia markers was necessary to delineate between cilia and acetyl-tubulin at the midbodies of dividing cells (Fig 3R). Importantly, no change in cilia number occurred when AKAP220-ΔPP1 cells were treated with tubacin (Fig 3S-Y). Similarly, AKAP220KO cells were unresponsive to the drug (Supp Fig 3D-G). This raises the intriguing possibility that an HDAC6-PP1-AKAP220 signaling axis is the intracellular target for the drug tubacin (Fig 3Z).

Figure 3

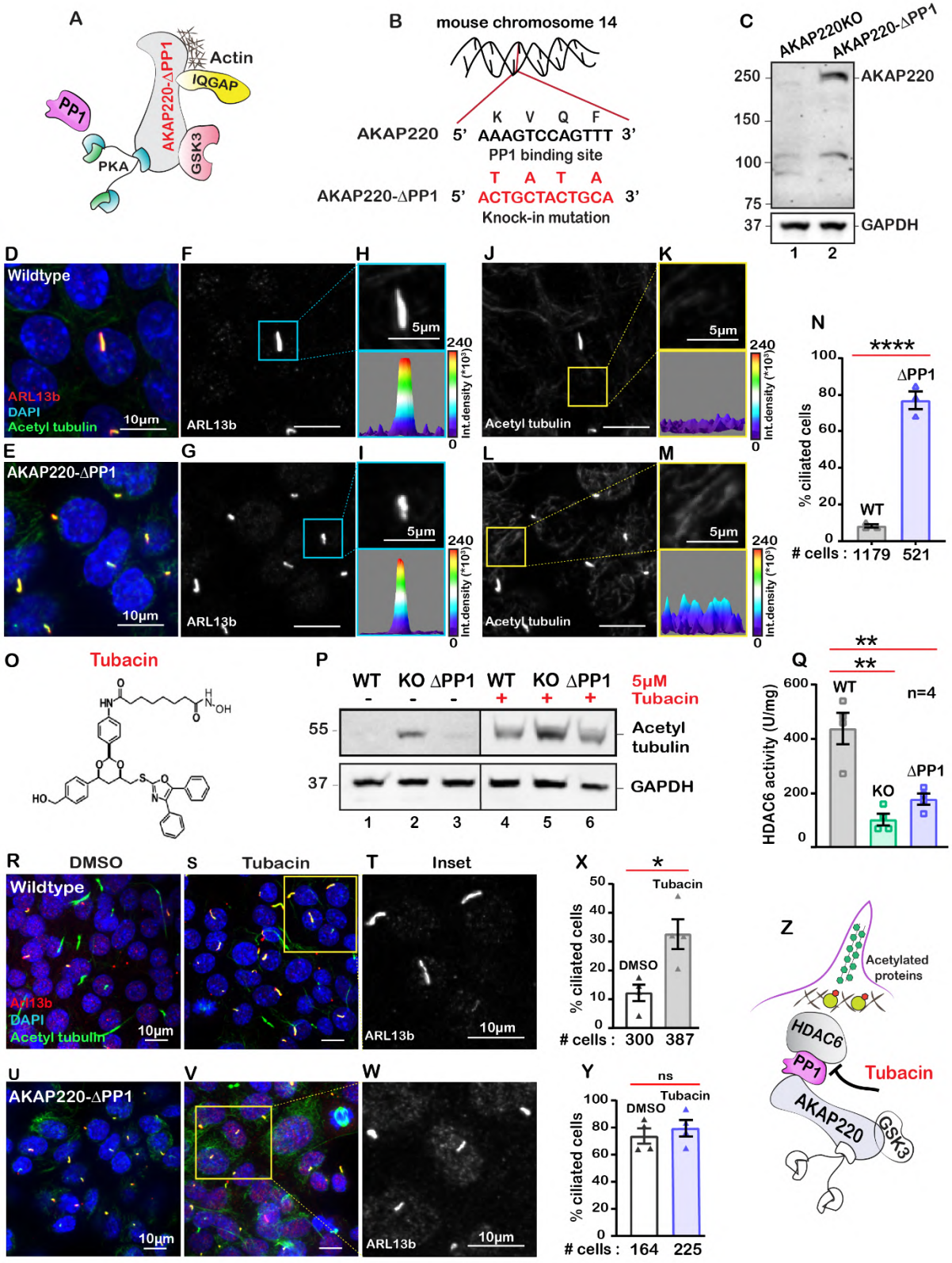
A
Actin
IQGAP
AKAP220-ΔPP1
PP1
PKA
GSK3
B
mouse chromosome 14
K V Q F
AKAP220 5' AAAGTCCAGTTT 3'
PP1 binding site
T A T A
AKAP220-ΔPP1 5' ACTGCTACTGCA 3'
Knock-in mutation
C
AKAP220KO
AKAP220-ΔPP1
250
150
100
75
37
AKAP220
GAPDH
1 2
D
Wildtype
ARL13b
DAPI
Acetyl tubulin
10μm
F
ARL13b
H
5μm
240
Int.density (*10³)
0
J
Acetyl tubulin
K
5μm
240
Int.density (*10³)
0
E
AKAP220-ΔPP1
10μm
G
ARL13b
I
5μm
240
Int.density (*10³)
0
L
Acetyl tubulin
M
5μm
240
Int.density (*10³)
0
N
****
ΔPP1
100
80
60
40
20
0
% ciliated cells
WT
cells : 1179 521
O
Tubacin
HN
O
H
N
OH
O
HO
O
O
S
O
N
P
WT KO ΔPP1 WT KO ΔPP1
5μM Tubacin
- - - + + +
55
Acetyl tubulin
37
GAPDH
1 2 3 4 5 6
Q
**
**
HDAC6 activity (U/mg)
600
400
200
0
WT
n=4
KO
ΔPP1
R
DMSO
Wildtype
Arl13b
DAPI
Acetyl tubulin
10μm
S
Tubacin
T
Inset
ARL13b
10μm
X
*
Tubacin
50
40
30
20
10
0
% ciliated cells
DMSO
cells : 300 387
Z
Acetylated proteins
HDAC6
PP1
Tubacin
AKAP220
GSK3
U
AKAP220-ΔPP1
10μm
V
W
ARL13b
10μm
Y
ns
Tubacin
100
80
60
40
20
0
% ciliated cells
DMSO
cells : 164 225

Figure 3: Anchored protein phosphatase 1 is necessary for HDAC6 activity

A) Schematic of AKAP220-ΔPP1. Binding partners are indicated. Gene editing deleted the principal phosphatase binding site (KVQF) on AKAP220. **B**) Nucleotide sequencing reveals substitution of the KVxF motif. **C**) Immunoblot detection of AKAP220 (top) and GAPDH loading control (bottom) in AKAP220KO (lane 1) and AKAP220-ΔPP1 (lane 2) mIMCD3 cell lysates. **D-N**) Immunofluorescent detection of acetyl tubulin (green), Arl13b (red) and DAPI (blue) in **D**) wildtype and **E**) AKAP220-ΔPP1 cells. Grey scale images of Arl13b in **F**) wildtype and **G**) AKAP220-ΔPP1 cells. A single enlarged cilium (top) and corresponding three-dimensional surface plots (bottom) from **H**) wildtype and **I**) AKAP220-ΔPP1 cells. Grey scale images of acetylated tubulin in **J**) wildtype and **L**) AKAP220-ΔPP1 cells. Enlarged sections from **J & L** (top) and corresponding three-dimensional surface plots (bottom) from **K**) wildtype and **M**) AKAP220-ΔPP1 cells. **N**) Quantification (% ciliated cells) in wildtype (grey) and AKAP220-ΔPP1 (blue). ****p<0.0001, N=3. **O**) Chemical structure of HDAC6 inhibitor tubacin. **P**) Immunoblot detection of acetylated tubulin in control and tubacin-treated wildtype (lanes 1 and 4), AKAP220KO (lanes 2 and 5) and AKAP220-ΔPP1 (lanes 3 and 6) cells. **Q**) HDAC6 activity levels (A.U.) in wildtype (grey), AKAP220KO (green) and AKAP220-ΔPP1 (blue) cells as assessed by Bioline's activity assay. **p<0.01, N=4. **R-U**) Tubacin enhances ciliogenesis in the presence of native AKAP220. Wildtype mIMCD3 cells treated with **R**) DMSO or **S**) tubacin (2μM) for 4 hrs. Immunofluorescent staining with acetyl tubulin (green), Arl13b (red) and DAPI (blue). **T**) Higher magnification grey scale image of Arl13b staining. **U**) Quantification (% ciliated cells) in DMSO (white) and tubacin-treated (grey) wildtype cells. *p<0.05, ns=non-significant; N=3. **V-Y**) Tubacin has no effect on AKAP220-ΔPP1 cells. **V**) DMSO or **W**) and **X**) tubacin treated AKAP220-ΔPP1 cells. **Y**) Quantification (% ciliated cells) and analysis as described above in DMSO (white) and tubacin-treated (blue). **Z**) Schematic of proposed tubacin mechanism of action on AKAP220-signaling complex. All error bars are s.e.m. *P* values were

calculated by unpaired two-tailed Student's t-test. Scale bars (10μm). Number of cells analyzed indicated below each column.

Figure 3 supplement

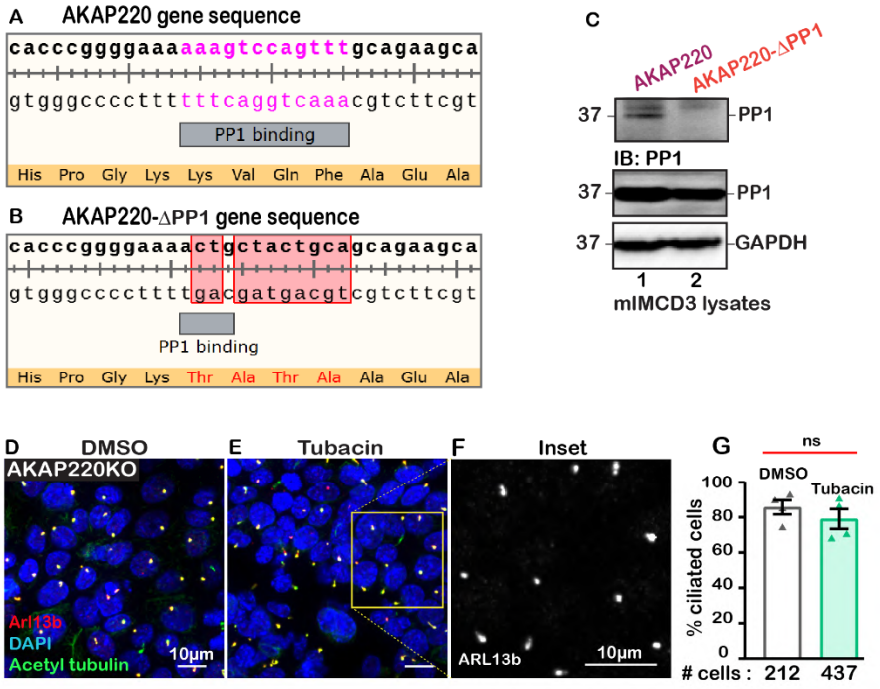

Supplemental figure 3: Further characterization of AKAP220-ΔPP1 and tubacin action.

CRISPR-Cas9 gene editing was used to substitute the PP1-targeting KVQF motif in AKAP220 gene to generate AKAP220-ΔPP1 mIMCD3 cells. Sequencing analysis data shows **A**) wildtype PP1-binding region in AKAP220 and **B**) modified TATA region in AKAP220-ΔPP1. **C**) Immunoprecipitation assay to validate AKAP220-ΔPP1 cells. Immunoblot detection of PP1(top panel) in AKAP220 immune complexes (lane 1), but not in AKAP220-ΔPP1 immune complexes (lane 2). mIMCD3 lysates are probed with PP1(mid) and GAPDH (lower) as loading control. Immunofluorescent staining with ciliary markers acetyl tubulin (green) and Arl13b (red) in **D**) DMSO and **E**) tubacin-treated AKAP220KO cells. DAPI (blue) serves as a nuclear marker. **F**)

Expanded grey scale image of Arl13b in tubacin-treated AKAP220KO cells. **G**) Quantification (% ciliated cells) in DMSO (black bar) and tubacin-treated (green bar) AKAP220KO cells. The number of cells analyzed from three independent experiments are indicated below the bar for each condition. ns=non-significant. Error bars are s.e.m. *P* values were calculated by unpaired two-tailed Student's t-test. Scale bars (10μm).

AKAP220 signaling impacts cortical actin dynamics.

The cytoskeleton maintains cell shape and structure by synchronizing the assembly and disassembly of actin, intermediate and tubulin filaments (Janke and Magiera, 2020; Klymkowsky, 1999). Covalent modification of these elements is an important facet of cytoskeletal regulation (Portran et al., 2017). For example HDAC6 deacetylates the actin-binding protein cortactin to relocate it from the nucleus to its sites of action (Ran et al., 2015). Since HDAC6 activity is impaired in AKAP220KO and AKAP220-ΔPP1 cells, it was important to evaluate if nuclear accumulation of acetylated cortactin was enhanced. Immunofluorescent detection of acetyl-cortactin (green) was more prominent in the nuclei of AKAP220KO and AKAP220-ΔPP1 mIMCD3 cells, as compared to wildtype (Fig 4A, C & E). This is emphasized in insets and corresponding surface plots (Fig 4B, D & F). Amalgamated data from three experiments are presented (Fig 4G). Next, we investigated if AKAP220 signaling influences actin filament morphology (Fig 4H-M). Immunofluorescent analyses show that AKAP220KO and AKAP220-ΔPP1 cells exhibit dramatic changes in the actin cytoskeleton (red) (Fig 4H, J & L). Line plot analyses (40-50 cells) reveal that total loss of the anchoring protein or disruption of HDAC6-PP1 attachment correlates with enhanced accumulation of cortical actin (Fig 4I, K & M). These findings pointed towards defects in actin dynamics.

To further explore this concept, we performed Fluorescence Recovery after Photobleaching (FRAP) at cell-cell junctional actin fibers (Mov 1-3). Actin-GFP recovery upon photobleaching was monitored over a time course of 20 seconds in wildtype (grey; Fig 4N); AKAP220KO (green; Fig 4O) and AKAP220-ΔPP1(blue; Fig 4P) mIMCD3 cells. Recovery curves depict the half-life and mobile fraction (Fig 4Q). Expanded section accentuates the expedited recovery of actin in wildtype cells (Fig 4Q, inset). The t1/2 for photo-recovery is 1.6 sec; n=106 (Fig 4R, grey). In contrast, the t1/2 was 0.9 sec; n=144 for AKAP220KO cells (Fig 4R, green). This is a 0.72 sec ±0.09 reduction in the rate of photo-recovery when compared to wildtype. Parallel FRAP experiments in AKAP220-ΔPP1 cells calculated a t1/2 of 1.75 sec; n=128, representing a 0.85 ± 0.10 sec reduction in the rate of photo-recovery as compared to wildtype (Fig 4R, blue). The availability of actin-GFP was similar in mobile fractions from each cell type (wildtype 95% (grey); AKAP220KO 98% (green); AKAP220-ΔPP1 98% (blue); Figure 4S). Thus, disruption of AKAP220-signaling impacts the distribution and dynamics of actin filaments.

Figure 4

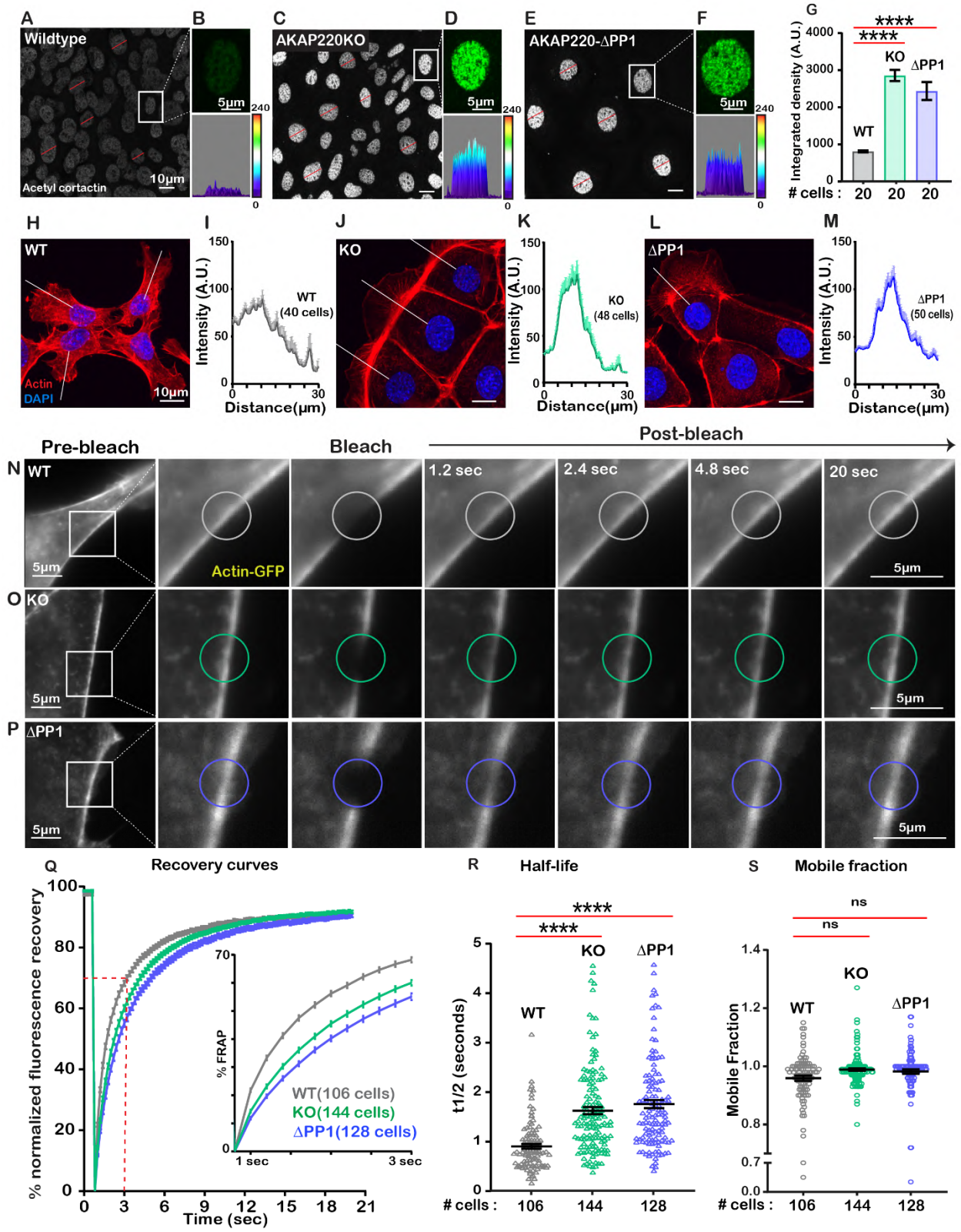
A
Wildtype
Acetyl cortactin
10μm
B
5μm
240
0
C
AKAP220KO
D
5μm
240
0
E
AKAP220-ΔPP1
F
5μm
240
0
G
****
****
Integrated density (A.U.)
4000
3000
2000
1000
0
WT
KO
ΔPP1
cells :
20
20
20
H
WT
Actin
DAPI
10μm
I
Intensity (A.U.)
150
100
50
0
WT
(40 cells)
0
30
Distance(μm)
J
KO
K
Intensity (A.U.)
150
100
50
0
KO
(48 cells)
0
30
Distance(μm)
L
ΔPP1
M
Intensity (A.U.)
150
100
50
0
ΔPP1
(50 cells)
0
30
Distance(μm)
Pre-bleach
Bleach
Post-bleach
N
WT
5μm
Actin-GFP
1.2 sec
2.4 sec
4.8 sec
20 sec
5μm
O
KO
5μm
5μm
P
ΔPP1
5μm
5μm
Q
Recovery curves
% normalized fluorescence recovery
100
80
60
40
20
0
0
3
6
9
12
15
18
21
Time (sec)
% FRAP
70
0
1 sec
3 sec
WT(106 cells)
KO(144 cells)
ΔPP1(128 cells)
R
Half-life
****
****
t1/2 (seconds)
5
4
3
2
1
0
WT
KO
ΔPP1
cells :
106
144
128
S
Mobile fraction
ns
ns
Mobile Fraction
1.4
1.2
1.0
0.8
0.7
0.0
WT
KO
ΔPP1
cells :
106
144
128

Figure 4: Loss of AKAP220-PP1 subcomplex impacts actin reorganization.

Grey scale images of acetylated cortactin in **A**) wildtype, **C**) AKAP220KO and **E**) AKAP220-ΔPP1 mIMCD3 cells. Magnified images of nuclei (top) and three-dimensional surface plots (bottom) of acetylated cortactin in **B**) wildtype, **D**) AKAP220KO and **F**) AKAP220-ΔPP1 cells. **G**) Quantification of amalgamated data (20 cells) from wildtype (grey), AKAP220KO (green) and AKAP220-ΔPP1 (blue) cells. ****p<0.0001, N=3. Scale bars (10μm). **H-M**) Confocal images of actin (red) and DAPI (blue) in **H**) wildtype, **J**) AKAP220KO and **L**) AKAP220-ΔPP1 cells. Lines indicate sites of line plot analysis to measure actin distribution from nuclei to the lamellipodia in **I**) wildtype (grey), **K**) AKAP220KO (green) and **M**) AKAP220-ΔPP1 (blue) cells. Scale bars (10μm). **N-S**) Fluorescence recovery after photobleaching (FRAP) in mIMCD3 cells. Time course (0-20 sec) of GFP-actin imaging in **N**) wildtype, **O**) AKAP220KO and **P**) AKAP220-ΔPP1 cells. **Expanded section**) Photobleached portion of cortical actin. **Q**) FRAP curves in wildtype (grey), AKAP220KO (green) and AKAP220-ΔPP1(blue) cells. **Inset**) Photo recovery rates over the first 3 seconds. **R**) The t1/2 value for each cell analyzed is presented for wildtype (grey), AKAP220KO (green) and AKAP220-ΔPP1(blue) cells. ****p<0.0001, N=3. **S**) The mobile fraction of each cell analyzed is presented for wildtype (grey), AKAP220KO (green) and AKAP220-ΔPP1(blue circles) cells. Non-significant, N=3. Scale bars (5μm). All error bars are s.e.m. *P* values were calculated by unpaired two-tailed Student's t-test. Number of cells analyzed indicated below each column.

Actin polymerization dictates cilium biogenesis and length.

Actin is a key regulator of cilia formation and elongation (Kim et al., 2015). AKAP220$^{-/-}$ mice exhibit reduced accumulation of apical actin through the diminished GTP-loading of RhoA (Whiting et al., 2016). This key regulator of cytoskeletal reorganization contributes to the

assembly of actin barriers in renal cells (Blattner et al., 2013). HDAC6-mediated stimulation of actin polymerization is a prerequisite for the disassembly of primary cilia (Ran et al., 2015). A convergence of these ideas hypothesizes that defective AKAP220-signaling alters the dynamics of the actin barrier assembly to enhance ciliation (Fig 5A).

To test this hypothesis, we treated wildtype cells with the actin-depolymerizing drug Cytochalasin D (Fig 5B-E). Drug application (200nM) for 4 h favored disassembly of actin (white) as monitored by immunofluorescence (Fig 5B & D). Cytochalasin D promoted a 2.95-fold increase in the percentage of ciliated cells (Fig 5F, pink column). Similar effects were observed in AKAP220KO cells (Fig 5G-L). These pharmacological effects were scored by measuring the length of cilia (Fig 5M, pink). Insets feature representative cilia at higher magnification (Fig 5I & L, upper panels). Three-dimensional surface plots depict drug-induced changes in cilia length (Fig 5I &L, lower panels). Thus, pharmacological blockade of actin assembly augments ciliogenesis. This effect is enhanced in AKAP220 null cells.

Jasplakinolide is a macrocyclic peptide that stabilizes f-actin and augments the formation of actin barriers (Holzinger, 2009). Drug treatment (500nM) for 1.5 h enhanced detection of cortical actin (white) and decreased the number of ciliated cells (pink; Fig 5N-S). Insets feature representative cilia at higher magnification (Fig 5P & S, upper panels). Three-dimensional surface plots depict drug-induced changes in cilia length (Fig 5P & S, lower panels). Collectively, these pharmacological studies show that bi-directional modulation of actin dynamics directly affects ciliation.

Figure 5

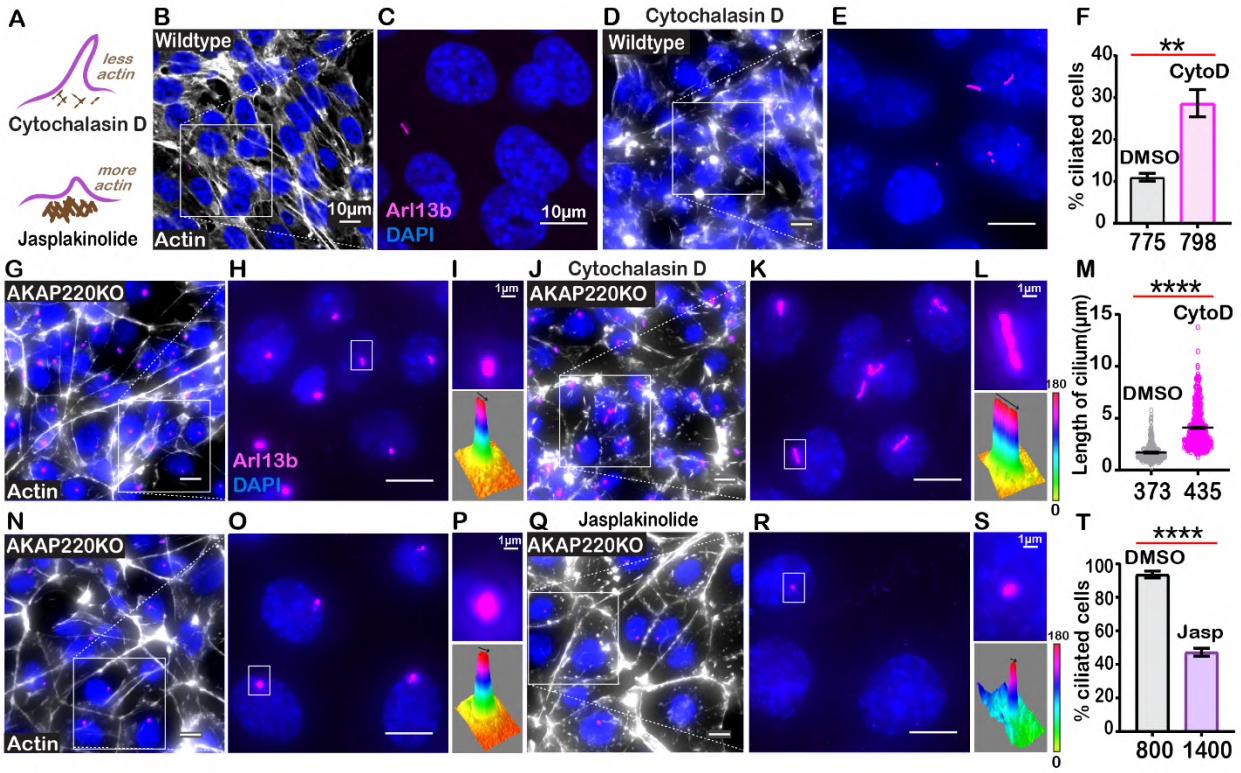

Figure 5: Cilia frequency and development are f-actin dependent.

A) Schematic of how actin modulating drugs impact primary cilia. Cytochalasin D depolymerizes actin barriers. Jasplakinolide stabilizes actin filaments. **B-F**) Immunofluorescent detection of actin (white), Arl13b (pink) and DAPI (blue) in wildtype mIMCD3 cells treated with **B**) DMSO or **D**) 200nM Cytochalasin D. Enlarged regions emphasize cilia frequency in **C**) DMSO and **E**) Cytochalasin D-treated cells. **F**) Quantification (% ciliated cells) in DMSO (grey) and Cytochalasin D (pink) treated cells. **p<0.01, N=3. **G-M**) Immunofluorescent detection of actin (white), Arl13b (pink) and DAPI (blue) in **G**) DMSO and **J**) Cytochalasin D treated AKAP220KO cells. **Inset)** Expanded field of cells treated with **H**) DMSO or **K**) Cytochalasin D. Boxed regions in **I** and **L** focus on a single cilium (top) and three-dimensional surface plot (bottom). The black arrow in the 3D surface plot represents cilium length. **M**) Quantification of cilia length in DMSO (grey) and Cytochalasin D (pink) treated cells. ****p<0.0001, N=3. **N-T**) Immunofluorescent

staining of actin (white) and DAPI (blue) of **N** (DMSO) and **Q** (Jasplakinolide) treated AKAP220KO cells. **Inset**) Expanded field of cells treated with **O**) DMSO or **R**) Jasplakinolide. Boxed regions in **P** and **S** focus on a single cilium (top) and three-dimensional surface plot (bottom). The width of the cylindrical region in the 3D surface plot represents cilium length. **T**) Quantification (% ciliated cells) in DMSO (grey) and Jasplakinolide (purple). ****p<0.0001, N=3. All error bars are s.e.m. *P* values were calculated by unpaired two-tailed Student's t-test. Scale bars (10μm). Number of cells analyzed indicated below each column.

Figure 5 supplement

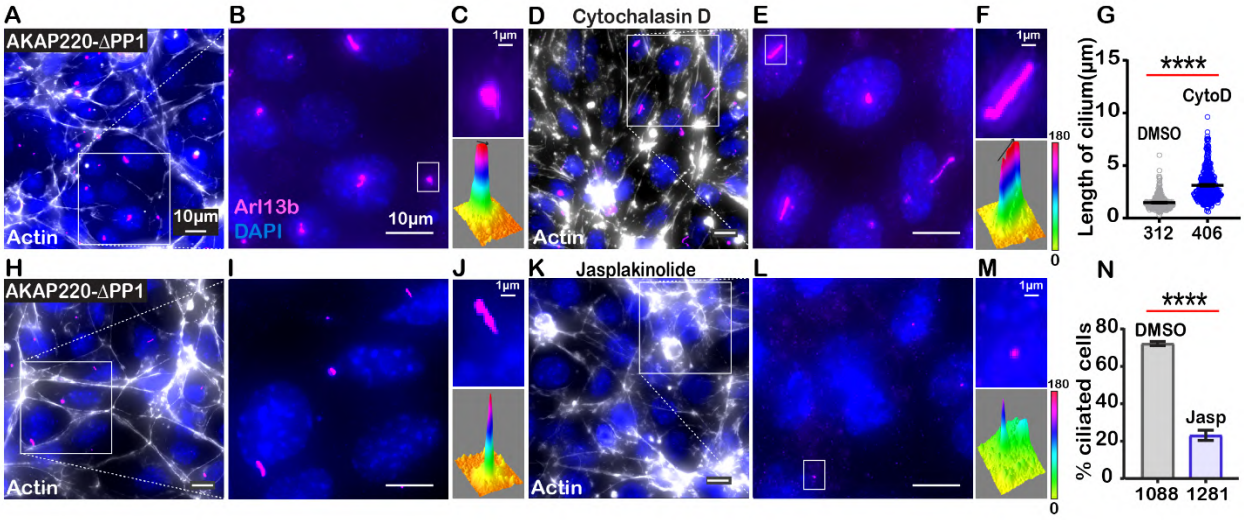

Supplemental figure 5: Characterizing the effect of actin-modulating drugs on AKAP220-ΔPP1 cilia.

A-G) Immunofluorescent detection of actin (white), Arl13b (pink) and DAPI (blue) in **A**) DMSO and **D**) 200nM Cytochalasin D-treated AKAP220-ΔPP1 mIMCD3 cells. **Inset)** Expanded field of cells treated with **B**) DMSO or **E**) Cytochalasin D. Boxed regions in **C** and **F** focus on a single cilium (top) and three-dimensional surface plot (bottom). The black arrow in the 3D surface plot represents cilium length. **G**) Quantification of cilia length in DMSO (grey) and Cytochalasin D (pink) treated cells. ****p<0.0001, N=3. **H-N**) Immunofluorescent staining of actin (white) and DAPI (blue) of **H** (DMSO) and **K** (Jasplakinolide) treated AKAP220-ΔPP1 cells. **Inset**) Expanded field of cells treated with **I**) DMSO or **L**) Jasplakinolide. Boxed regions in **J** and **M** focus on a single cilium (top) and three-dimensional surface plot (bottom). The width of the cylindrical region in the 3D surface plot represents cilium length. **N**) Quantification (% ciliated cells) in DMSO (grey) and Jasplakinolide (purple). ****p<0.0001, N=3. All error bars are s.e.m. *P* values were calculated by unpaired two-tailed Student's t-test. Scale bars (10μm). Number of cells analyzed indicated below each column.

AKAP220 signaling influences cilia morphology.

We reasoned that a consequence of altered actin dynamics could be changes in cilia morphology. Super-resolution immunofluorescence imaging of fixed cells was performed using Arl13b as a ciliary marker. Cilia appeared retracted in AKAP220-null and ΔPP1-knock in cells in comparison to cylindrical and symmetrical architecture of cilia in wildtype cells (Fig 6A-D). A secondary feature was bulbous tips at the distal end of mutant cilia (Fig 6C & D). Analyses from three independent experiments show that the occurrence of bulbous tips was prevalent in cilia from AKAP220KO and AKAP220-ΔPP1 cells (Fig 6E).

To investigate this phenomenon further in living cells, we infected our mIMCD3 cell lines with a lentiviral vector encoding Arl13b-GFP (Mov 4-6; Fig 6F-H). Quantitative imaging by live-cell super-resolution microscopy revealed that cilia in AKAP220KO (green) and AKAP220-ΔPP1 (blue) cells were 1.6 and 1.7-fold longer than wildtype counterparts (grey; Fig 6H). This led us to the conclusion that the bulbous tips presented in figures 6C & D were elongated, flexible cilia that partially retracted (coiled back) on themselves (Supp Fig 6).

Kidney-on-a-chip technology offers a pseudo-physiological environment that simulates kidney tubules (Weber et al., 2016). Microfluidic delivery of nutrients through the lumen of these tubules recapitulates fluid-flow (Freedman et al., 2013). This sophisticated tissue-engineering approach was used to evaluate cilia development (Fig 6I). Culturing of wildtype mIMCD3 cells formed columnar organoids with few cilia protruding into the lumen (Fig 6J & K). In contrast, more cilia were evident in AKAP220-ΔPP1 organoids (Fig 6L & M). Immunofluorescent staining of Arl13b (red) and acetyl tubulin (green) marked cilia and DAPI (blue) detected nuclei. The average cilia length was 3.95-fold greater in AKAP220-ΔPP1 pseudo-tubules (n=73 cilia) as compared to

wildtype (n=53 cilia). These effects are more visible in the grey scale images of Arl13b alone (Fig 6L). Amalgamated data from three independent experiments are presented in figure 6I.

Cilia assembly requires the passage of materials through an actin barrier formed across the basal body (Farina et al., 2016). We reasoned that the dynamics of this process may be altered upon manipulation of AKAP220 signaling. Therefore, we combined super-resolution microscopy with Fluorescence Recovery after Photobleaching (FRAP) to visualize GFP-Arl13b trafficking into individual cilia (Fig 6N). Arl13b recovery upon photobleaching was monitored over a time course of 2.5 seconds in wildtype (grey; Fig 6P); AKAP220KO (green; Fig 6Q) and AKAP220-ΔPP1(blue; Fig 6R) mIMCD3 cells. In wildtype cells, the rate of GFP-Arl13b recovery was steady over this time-course. FRAP was more rapid and robust in AKAP220KO and AKAP220-ΔPP1 cilia (Fig 6S). Total Arl13b recovered in AKAP220KO is increased 22.35 ±3% (n= 120 cilia; green; Fig 6T) over wildtype (n=60 cilia; grey; Fig 6T). Similarly, recovery of Arl13b in AKAP220-ΔPP1 cilia is 19.04 ±3% increased (n=126 cilia; blue; Fig 6T) over wildtype. The t1/2 of Arl13b recovery was 178.9 milliseconds in wildtype cilia (grey), as compared to 344.7 and 361.6 milliseconds in AKAP220KO and AKAP220-ΔPP1 cilia respectively (Fig 6U; green and blue). These studies suggest that there is a larger mobile pool of Arl13b trafficking into the mutant cilia. One plausible mechanism is that cilia in AKAP220KO and AKAP220-ΔPP1 cells lack an architectural checkpoint that gates protein movement into this organelle. A likely candidate is an f-actin barrier at the base of the cilium (Fig 6V).

Figure 6

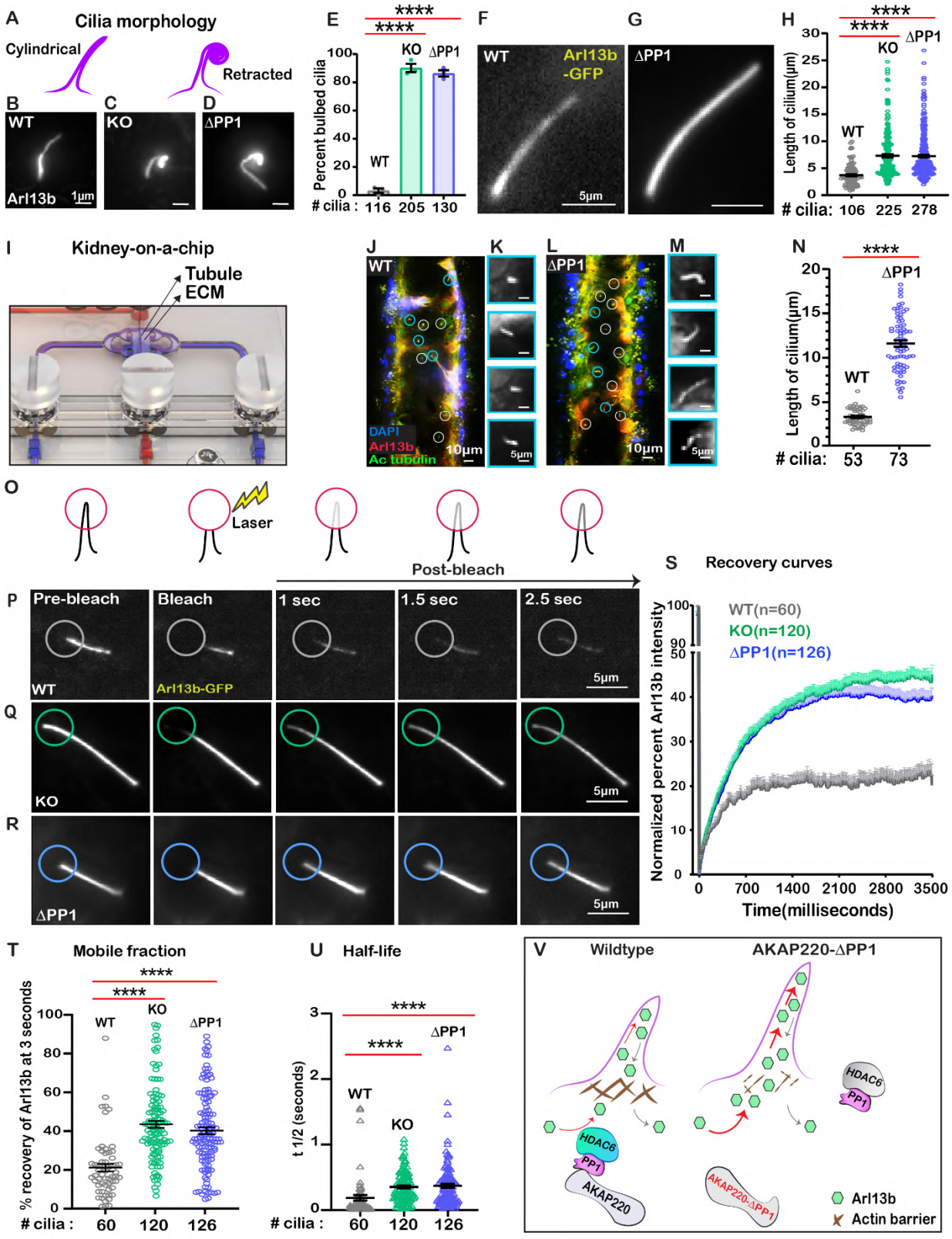
A
Cilia morphology
Cylindrical
Retracted
B
WT
Arl13b
1μm
C
KO
D
ΔPP1
E
****
****
Percent bulbed cilia
100
80
60
40
20
0
WT
KO
ΔPP1
cilia : 116 205 130
F
WT
Arl13b
-GFP
5μm
G
ΔPP1
H
****
****
ΔPP1
KO
WT
Length of cilium(μm)
30
25
20
15
10
5
0
cilia: 106 225 278
I
Kidney-on-a-chip
Tubule
ECM
J
WT
DAPI
Arl13b
Ac tubulin
10μm
K
5μm
L
ΔPP1
10μm
M
5μm
N
****
ΔPP1
WT
Length of cilium(μm)
20
15
10
5
0
cilia: 53 73
O
Laser
Post-bleach
P
Pre-bleach
Bleach
1 sec
1.5 sec
2.5 sec
WT
Arl13b-GFP
5μm
Q
KO
5μm
R
ΔPP1
5μm
S
Recovery curves
WT(n=60)
KO(n=120)
ΔPP1(n=126)
Normalized percent Arl13b intensity
100
90
50
40
30
20
10
0
0
700
1400
2100
2800
3500
Time(milliseconds)
T
Mobile fraction
****
****
% recovery of Arl13b at 3 seconds
100
80
60
40
20
0
WT
KO
ΔPP1
cilia : 60 120 126
U
Half-life
****
****
t 1/2 (seconds)
3
2
1
0
WT
KO
ΔPP1
cilia : 60 120 126
V
Wildtype
AKAP220-ΔPP1
HDAC6
PP1
AKAP220
AKAP220-ΔPP1
HDAC6
PP1
Arl13b
Actin barrier

Figure 6: Loss of phosphatase anchoring promotes cilium elongation.

A) Schematic of cylindrical and retracted cilia morphologies (purple). Super-resolution fixed-cell imaging of Arl13b (grey scale) in **B**) wildtype, **C**) AKAP220KO and **D**) AKAP220-ΔPP1 cilia. **E**) Quantification (% bulbed cilia) in wildtype (grey), AKAP220KO (green) and AKAP220-ΔPP1 (blue) cells. ****p<0.0001, N=3. Scale bars (1μm). Super-resolution live-cell images of Arl13b-GFP in **F**) wildtype and **G**) AKAP220-ΔPP1 cilia. **H**) Quantification of cilia length in wildtype (grey), AKAP220KO (green) and AKAP220-ΔPP1 (blue) cells. ****p<0.0001, N=3. Scale bars (5μm). **I**) Kidney-on-a-chip device. Location of kidney tubule (Tubule) and extracellular matrix (ECM) are indicated. Confocal imaging of **J**) Wildtype and **L**) AKAP220-ΔPP1cells cultured in chip device with Arl13b (red), acetyl tubulin (green) and DAPI (blue). Cilia (white circles) are marked. **Insets**) Magnified images of representative cilia (cyan circles) from **K**) wildtype and **M**) AKAP220-ΔPP1 pseudotubules. **N**) Quantification of cilia length in wildtype (grey) and AKAP220-ΔPP1 (blue). ****p<0.0001, N=3. Scale bars (10μm). Inset scale bars (5μm). **O-U**) Fluorescence recovery after photobleaching (FRAP) of Arl13b-GFP in primary cilia. **O**) Schematic of how FRAP was measured. **P-R**) Super-resolution live-cell images of Arl13b-GFP in **P**) wildtype, **Q**) AKAP220KO and **R**) AKAP220-ΔPP1 cells. Circles mark bleached portion of cilia. **S**) FRAP recovery curves of Arl13b over time (3500 milli sec) in wildtype (grey), AKAP220KO (green) and AKAP220-ΔPP1 (blue) cells. Scale bars (5μm). **T**) Quantification of mobile fraction in wildtype (grey), AKAP220KO (green) and AKAP220-ΔPP1 (blue) cilia. ****p<0.0001, N=3. **U**) Half-life of Arl13b in wildtype (grey), AKAP220KO (green) and AKAP220-ΔPP1 (blue) cilia. ****p<0.0001, N=3. **V**) Schematic depicting how AKAP220 modulation of the actin barrier influences movement of proteins in and out of primary cilia. All error bars are s.e.m. *P* values were calculated by unpaired two-tailed Student's t-test. Number of cilia analyzed indicated below each column.

Figure 6 supplement

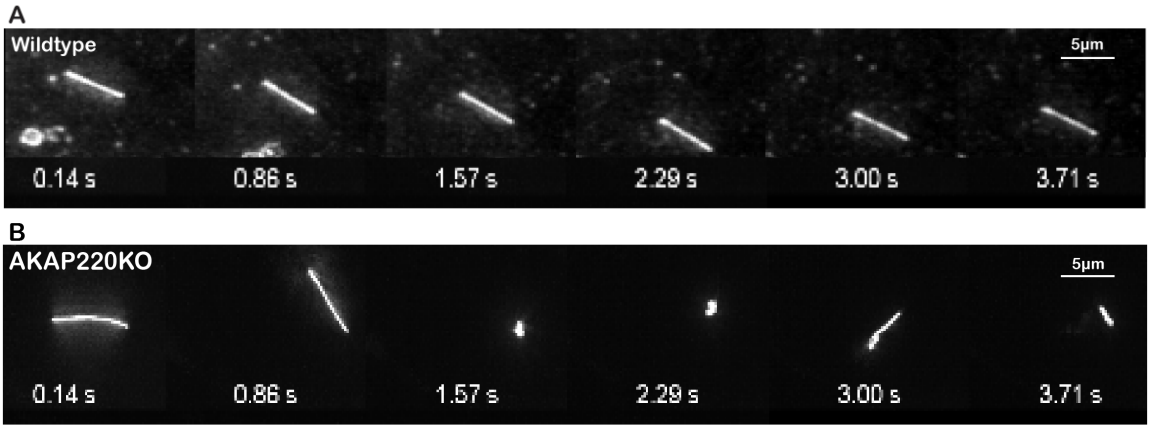

Supplemental figure 6: Super resolution videos depicting flexibility of AKAP220KO cilia.

A) Wildtype and **B**) AKAP220KO primary cilia from mIMCD3 cells transduced with Arl13b-GFP were monitored across a time course of 4 seconds. The AKAP220 cilium is longer and more flexible compared to the wildtype.

HDAC6 inhibition attenuates renal cyst formation.

Autosomal dominant polycystic kidney disease (ADPKD) is associated with mutations in *PKD1* and *PKD2,* changes in apical actin and cilia dysfunction (Halvorson et al., 2010). This pathology is characterized by fluid-filled cysts that replace normal renal parenchyma (Fig 7A). Aberrant HDAC6 activity has been implicated in cyst growth (Sun et al., 2019). Therefore, we reasoned that pharmacologically targeting HDAC6 may have therapeutic benefit in the reduction of cyst formation in cellular models of ADPKD (Fig 7B). Human pluripotent stem cells (hPSCs) with a targeted disruption of *PKD2* were differentiated into kidney organoids (Freedman et al., 2015). Cysts were identified as large, translucent structures that swayed in response to agitation (Fig

7C & D). *PKD2*$^{-/-}$ kidney organoids and matched isogenic controls were treated with tubacin (0.2-1μM) for 48 h and cyst size was evaluated. At low concentrations of tubacin (0.2 μM), renal cyst size was markedly reduced in *PKD2*$^{-/-}$ organoids as compared to the control (Fig 7E & F). Similar results were obtained at a higher dose of 1μM (Fig 7G & H). Amalgamated data from five experiments are presented (Fig 7I). Drug toxicity as assessed by luminescence assay was evident at higher doses of tubacin (Fig 7J). Thus, pharmacologically targeting the AKAP220-binding partner HDAC6 reduces cystogenesis in a disease relevant model of ADPKD.

Figure 7

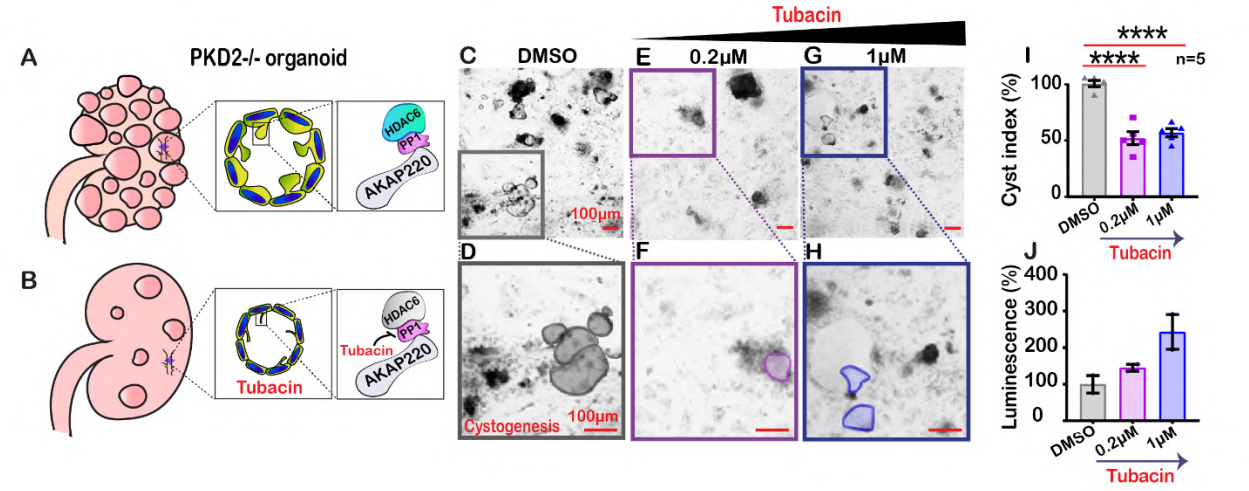

Figure 7: Inactivating HDAC6 reduces renal cystogenesis.

Schematic of polycystic kidneys **A**) before and **B**) after tubacin treatment. **Insets**) Tubacin action on the AKAP220-signaling complex in precystic PKD2$^{-/-}$ organoids derived from WA-09 cells. **C-J**) Confocal images of PKD2$^{-/-}$ organoids treated with **C**) DMSO, **E**) 0.2 μM and **G**) 1μM tubacin. Enlarged regions from **C, E** and **G** showing cysts in **D**) DMSO, **F**) 0.2 μM and **H**) 1μM tubacin-treated conditions. Scale bars (100μm). **I**) Quantification (% cyst index) in DMSO (grey), 0.2 μM (purple) and 1μM (blue) tubacin-treated conditions. ****p<0.0001, N=5. **J**) Luminescence assay to detect toxicity of the drug is plotted for DMSO (grey), 0.2 μM (purple) and 1μM (blue)

tubacin-treated conditions. Error bars are s.e.m. *P* values were calculated by unpaired two-tailed Student's t-test.

Discussion

The primary cilium is a highly organized mechanosensory transduction unit that responds to environmental cues (Goetz and Anderson, 2010; Wheway et al., 2018). We have discovered signaling events proceeding through AKAP220 that temper cilia development in kidney collecting ducts. While it may seem paradoxical that disruption of local signaling can positively impact organellar development, it is important to note that a few AKAPs mitigate signaling events in other cellular contexts (Bucko and Scott, 2021; Langeberg and Scott, 2015). At neuronal synapses, tonic phosphatase activity constrained by AKAP79/150 attenuates the phosphorylation status and activity of excitatory ionotropic glutamate receptors that contribute to learning and memory (Hoshi et al., 2005; Tunquist et al., 2008). In cardiomyocytes, AKAP18 anchored phosphodiesterase-3 degrades cAMP that sustains excitation-contraction coupling (Lygren et al., 2007). Likewise, AKAP220 binding partners repress aquaporin-2 shuttling to apical membranes of kidney collecting ducts to maintain renal water homeostasis (Whiting et al., 2016).

Our imaging analysis of tissue sections from AKAP220$^{-/-}$ mice and cell lines indicate that loss of this anchoring protein enhances cilia development. Interestingly, AKAP79/150 has been implicated as a modulator of renal ciliary signaling (Choi et al., 2011). However, proximity proteomic approaches identify AKAP220 in cilia, and knockout of the AKAP79/150 ortholog in mIMCD3 cells and mice has no effect on cilia development ((May et al., 2020) & Supp Fig 1). Although we cannot exclude AKAP79/150 as a local mediator of certain ciliary events, our *in vivo* and *in vitro* data strongly implicate AKAP220 signaling in the modulation of aquaporin-2

trafficking and ciliogenesis. This could occur through one of two mechanisms- either the cellular signals that attenuate aquaporin-2 trafficking and diminish cilia development are processed through the same macromolecular complex, or, distinct signaling islands of AKAP220-binding partners are assembled to control each process.

A unifying principle of our study is that AKAP220-binding partners affect the development of primary cilia by enacting cytoskeletal changes at the level of actin polymerization and tubulin acetylation. This implicates deacetylation as a fundamental signal termination process that checks the rate of cilia development. Histone deacetylase 6 (HDAC6) that targets the cytoskeletal elements alpha tubulin and cortactin has been identified as a driver of cilia disassembly (Ran et al., 2015). In keeping with this notion, data in figure 2Q show that rescue upon overexpression of HDAC6 in an AKAP220KO background restores control of ciliation. Several lines of evidence suggest a role for AKAP220 in this process. Data in figure 2 indicate that this deacetylase is more labile in the absence of the anchoring protein. While phosphorylation protects HDAC6 from ubiquitination, and dephosphorylation favors proteasomal degradation, it has been unclear how this enzyme is maintained in proximity of developing cilia (Ran et al., 2020). Our findings point towards a previously unrecognized adaptor function for protein phosphatase 1 (PP1). This reasoning is predicated on evidence that AKAP220 is a conventional PP1-targeting subunit that utilizes a KVxF motif to contact the phosphatase (Bollen et al., 2010).

While the mechanism of HDAC6 interaction with PP1 is less clear (Brush et al., 2004), it appears that the anchored phosphatase retains the capacity to function as an adaptor protein and recruit this additional binding partner. This is inferred by pulse-chase data showing that HDAC6 protein stability is compromised in AKAP220KO cells and supported by proximity-ligation data detecting HDAC6 in AKAP220-signaling islands (Fig 2I-O). Thus, AKAP220-PP1

subcomplexes create a platform for the targeting of HDAC6 to repress tubulin acetylation during ciliogenesis. This may represent a homeostatic mechanism that enables cells to enter mitosis.

Mutations in the ciliary phosphoproteins polycystin 1 and 2 are linked to autosomal dominant polycystic kidney disease (ADPKD) (Hughes et al., 1995; Mochizuki et al., 1996; Streets and Ong, 2020). Trafficking of polycystin-1 to the ciliary membrane is dependent on local PP1 activity (Parnell et al., 2012). Likewise, bi-directional control of polycystin-2 channel conductance is modulated by an anchored PKA-PP1 component (Streets et al., 2013). Thus, local dephosphorylation events are key to the termination of mechanotransduction signals that govern primary cilia action in ADPKD. Using the AKAP220-ΔPP1 knock-in mutant as a mechanistic probe, we have uncovered a new non-catalytic role for anchored-PP1 in the regulation of cytoskeletal events that underlie renal cilia biogenesis. The striking changes observed in actin remodeling and cilia morphology presented in figures 4 and 5 can solely be attributed to disruption of the KVxF motif in AKAP220 (Schillace and Scott, 1999). Concomitant effects on HDAC6 location not only enhance cortactin acetylation, but also enact changes in actin dynamics.

Such cytoskeletal reorganization at defined sites is a prelude to cilia extension. Focal adhesion proteins attach the basal body to actin filaments (Drummond et al., 2018; Kim et al., 2015). This signals clearing of the local actin barrier to commence microtubule nucleation. In keeping with this notion, data in figure 5 show that the actin depolymerizing drug Cytochalasin D enhances cilia persistence and length, whereas the actin-stabilizing compound Jasplakinolide has the opposite effect (Casella et al., 1981; Holzinger, 2009). These pharmacological tools highlight the action of AKAP220-associated enzymes at the level of the actin barrier. This substructure is part

of a “ciliary necklace” that acts as a physical checkpoint for proteins moving into the cilium (Long and Huang, 2020). This is supported by photobleaching studies showing that Arl13b moves more readily in AKAP220-ΔPP1 mutant cilia and these organelles are approximately 2-fold longer than wildtype (Fig 6H). Thus, it is plausible that AKAP220-associated PP1 participates in maintenance of an actin barrier close to the basal body of the cilium, the loss of which leads to unhindered protein movement into the developing organelle.

Understanding the signaling mechanisms that govern primary cilia biogenesis in collecting ducts has potential for the treatment of autosomal dominant polycystic kidney disease. Our work points towards the AKAP220-PP1-HDAC6 signaling axis as a therapeutic target for this ciliopathy. Two lines of evidence converge on this notion. First, HDAC6 mediated deacetylation of tubulin controls cilia depolymerization. HDAC6 inhibitors including tubastatin A, ACY-1215 and tubacin are in early phase clinical trials to manage cancers and ciliopathies (Dong et al., 2018; Haggarty et al., 2003; Song et al., 2020). Our pharmacological studies now utilize tubacin to enhance ciliogenesis in wildtype mIMCD3 cells. Importantly, we show in figure 3Y that this selective-HDAC6 inhibitor has no effect in AKAP220-ΔPP1 cells. This argues that the AKAP220-PP1-HDAC6 axis is a molecular target for this drug. Consequently, tubacin could be exploited as a precision pharmaceutical to enhance ciliogenesis in disorders that arise from loss of primary cilia. Second, since HDAC6 activity is elevated in *PKD1* mutant renal epithelial cells (Li et al., 2016), we examined tubacin action in human cellular models of ADPKD. In figure 7, we show that tubacin reduced cystogenesis in *PKD2*$^{-/-}$ precystic organoids. Hence, targeting the AKAP220-PP1-HDAC6 subcomplex may not only enhance cilia development, but also interfere with downstream signaling events that contribute to cystogenesis. The AKAP-targeting concept has recently been used to restrain kinase inhibitor drugs at defined subcellular locations (Bucko et al., 2019, 2020). We will expand this approach towards developing a precision pharmacology

strategy to selectively deliver HDAC6 inhibitors to primary cilia for the treatment of chronic disorders such as polycystic kidney disease.

Materials and methods

Tissue section immunofluorescent staining

Kidneys were fixed in 10% (vol/vol) buffered formalin (4 °C), embedded in paraffin and 4-µm-thick sections collected. Sections were deparaffinized using Citrasolv (Fisher) and antigen retrieved in buffer A using a Retriever 2100 pressure cooker (Electron Microscopy Sciences). Tissue sections were blocked in 10% (vol/vol) donkey serum in PBS solution before overnight incubation with the respective primary antibodies.

mIMCD3 spheroids

mIMCD3 cells were seeded in Matrigel to generate spheroids as previously described (Giles et al., 2014). The spheroids were stained with Acetyl tubulin for marking primary cilia and those with a visible open lumen were imaged and used in the quantification.

Cell culture

mIMCD3 cells were maintained in DMEM: F12 1:1 media supplemented with 10% FBS and penicillin/streptomycin. Cells were transfected with plasmids using Mirus TransIT-LT1 transfection reagent and incubated for 48-72 hrs before lysis or fixation. All cell lines were maintained in a 5% CO2 incubator at 37 °C.

Virus generation

Constitutively active lentiviral plasmids expressing Arl13b-GFP were transfected into HEK cells along with viral packaging and envelope plasmids. The viral particles generated are filtered and

added to mIMCD3 cells. After 24 hours of incubation, the cells were selected in zeocin (400ug/ml) for the next 2 weeks. After selection, the cells were trypsinized and plated at a low density of about 1 cell/well in 96 well plate, expanded and tested for expression of Arl13b-GFP by western blotting and immunofluorescence.

Immunoblotting and blot analysis

Cells were grown to the desired confluence and washed once with PBS at room temperature. Cold lysis buffer (20 mM HEPES, (pH 7.4),150 mM NaCl,1 mM EDTA,1% triton X-100 in water) was added along with protease and phosphatase inhibitors and the plate was rocked gently at 4 degrees for 10 mins. The cell lysate was then scarped into a pre-chilled tube and cleared at 12,000*g for 10 min at 4 degrees. A BCA assay (Pierce) was used to determine protein concentrations, and 30µg of protein was loaded onto a Bolt 4–12% bis-Tris gel (Life Technologies). The cleared lysate was boiled in 2X SDS loading buffer for 10 min before loading. Proteins were transferred to nitrocellulose membrane and blocked in either 5% milk. The blot was incubated in primary antibody at 1:1000 or as specified by the manufacturer overnight at 4 °C. Immunoblots were washed (3 times, 10 mins each) in TBST before incubation in a 1:10,000 secondary antibody for 1 hr at room temperature. Immunoblots were washed again in TBST (3 times, 10 mins each) before imaging on an iBright FL1000 (Thermo Fisher Scientific) with SuperSignal Dura ECL reagent (Thermo Fisher Scientific). Densitometry for blot quantification was done using thermo fisher's software.

Immunofluorescence and microscopy

Sample preparation: Cells were seeded on acid-washed coverslips in 12-well plates. After they achieve the desired confluence, the wells were rinsed thrice with PBS and fixed with 4% paraformaldehyde in PBS or 10% ice cold methanol (based on the antibody specification) for 12 mins. After fixation, the cells were permeabilized in PBS+0.1%Triton x-100+1%BSA for 12 mins,

blocked with 2%BSA for 30 mins and treated with the respective primary antibodies overnight. After thorough washing in PBS the next day (3 times, 5mins each), secondary antibodies conjugated to Alexa fluor dyes were added for 2 hours. After 2 washes in PBS, DAPI along with or without the actin probe (based on the experiment) was added for 10 mins. The coverslips were washed 2 more times in PBS and mounted on slides using ProLong Diamond Antifade Mountant (Life Technologies).

Imaging and analysis: Cells were imaged on a Keyence BZ-X710 microscope (Keyence, Itasca, IL) using the relevant filter cubes for DAPI (blue filter), Actin (red filter), Cortactin (green filter). All images were acquired with the same magnification (100X, oil immersion), exposure time, and illumination intensity. Images were quantified and processed using ImageJ software.

FRAP (Fluorescence recovery after photobleaching)

Sample preparation: Cells were reverse transfected with lifeact-GFP (Addgene plasmid no.58470) and seeded into 60mm glass-bottom plates for 24 hours. The transfected plates are rinsed in PBS and incubated in Fluorobrite medium containing NucBlue Hoescht 33342 stain (R37605, Invitrogen, 1 drop/ml). For Arl13b FRAP, mIMCD3 lines were transduced with L13-Arl13bGFP lentiviral construct and selected as outlined above. These cells were seeded in 60mm glass-bottom plates. They were treated with 0.1%FBS for 24 hours and then the experiment was performed.

Imaging technique and analysis: Cells were imaged on a GE Deltavision OMX SR microscope (GE Life Healthcare Sciences). After loading (as above), cells were placed in a humidified chamber with 5% CO2 at 37 °C and imaged using a 60X oil immersion objective (Olympus, Shinjuku, Tokyo, Japan). The actin signal was photobleached in the green channel (488nm) using a 15% laser power for 0.05 seconds. A total of 5 events were captured before photobleaching. Images after photobleaching were captured every 100 milliseconds for 10

seconds. For Arl13b FRAP, Lentiviral Arl13b GFP mIMCD3 cells. The Laser pulse at 488 was at 30% T, in a spot at the tip of the cilium to bleach it for 0.1 seconds. 5 events before the bleach and a total of 350 time points were taken at 10msec increments. All images were acquired with the same settings. Images were quantified and processed using ImageJ software.

Antibodies

The following antibodies were used in this study for immunoblotting: AKAP220 (custom rabbit polyclonal,1:1000), GAPDH (Novus, mouse monoclonal, 1:5000), Acetylated tubulin (Thermo Fisher # 32-2700, 1:1000), HDAC6 (Proteintech # 12834-1-AP, 1:1000). Antibodies used for immunofluorescence: Acetylated tubulin (Thermo Fisher # 32-2700, 1:10000), HDAC6 (Proteintech, 12834-1-AP, 1:400), Arl13b (Proteintech # 17711-1-AP, 1:5000), Actin (Molecular probe, R37112, 1drop/ml).

Plasmids

Lentiviral Arl13b-GFP (# 40879) and lifeact-GFP (#58470) were purchased from addgene.

Statistics for all experiments

Statistical analysis was performed using an unpaired two-tailed Student's t-test or one-way ANOVA (based on the number of samples) in GraphPad Prism software. All values are reported as mean ± standard error of the mean (s.e.m) with p-values less than 0.05 considered statistically significant. For each experiment, number of independent experiments (N) and number of individual points from all experiments (n) are presented.

Line-plot analysis in ImageJ

For the actin and cortactin distribution experiments, lines were drawn from the outer edge of the nucleus to beyond the lamellipodia of the cell and line plots were generated using ImageJ to give the pixel intensity of each of the proteins along the line.

HDAC6 activity assay

The experiment was performed using BioVision's HDAC6 activity assay kit. mIMCD3 cells were seeded in 10cm dishes and allowed to grow for the desired confluence. They were then lysed using the lysis buffer provided in the kit. The protein concentration was measured using BCA assay kit (Pierce) and 20µg of protein was loaded per well. 5µM tubacin was used in the experiment and the fluorescence intensity was measured at 380/490 nm in the plate reader.

Drug treatment experiments

mIMCD3 cells were seeded on cover slips in 12-well plates and allowed to grow to the desired confluence. They were treated with 2uM tubacin for 4 hours, 200nM cytochalasin D for 4 hours or 500nM Jasplakinolide for 1.5 hours and fixed immediately after treatment (as previously described). The cells were stained for acetyl tubulin and Arl13b to mark primary cilia and DAPI to stain DNA.

Organoid differentiation

Organoids were differentiated in 384 well plates from human pluripotent stem cells (WTC11 iPS cells, Conklin lab, Gladstone Institute) that had been modified to disrupt *PKD2* (Cruz et al., 2017)

CHAPTER 4: AKAP220 regulates cell migration and adhesion

ABSTRACT

All cells rely on signaling systems to communicate with neighboring cells and the extracellular matrix. Proper coordination and and ensuring the fidelity of information transfer among cells are fundamental to organogenesis and physiology. Cell-cell contact is established by a group of proteins called cell adhesion molecules. Two classes of transmembrane receptors-integrins and cadherins are perhaps the best understood proteins that participate in cell adhesion. While integrins aid in cell-matrix adhesion via focal adhesions, cadherins enable cell-cell contact by forming adherens junctions (Parsons et al., 2010). Formation and release of focal adhesions are also important for cell movement and migration (Wozniak et al., 2004). Not surprisingly, loss of communication or poor communication between a cell and its environment leads to cancer metastasis and autoimmune disorders. Hence, this is an area of burgeoning research to understand the factors that drive proper communication and migration.

The co-existence of cell-cell junctions in adhesion and migration processes are driven by specific signaling pathways. The Rho small GTPase family comprised of Rho, Rac and Cdc42 regulate assembly, morphology, and maturation of cell-cell junctions (Lawson and Burridge, 2014). AKAP220 also interacts with the Rho-family GTPase effector protein IQGAP1 near the

cell cortex to positively regulate actin polymerization and microtubule stability during membrane protrusion and cell migration (Logue et al., 2011). Additionally, in my recent studies we find that this scaffolding protein also regulates localization and expression of E cadherin and β4 integrin at cell-cell and cell-matrix adhesion sites. Further, loss of AKAP220 enhances focal adhesion complex formation and cell spreading. These processes proceed through proper polymerization and distribution of actin, both of which are influenced by localization of kinases and phosphatases by AKAP220.

INTRODUCTION

Cell migration

Cell migration is a fundamental process involved in the development of multicellular organisms. Movement of cells in an orchestrated fashion drives embryonic development, wound healing, and immune responses (Lauffenburger and Horwitz, 1996). Given how central this process is, even the slightest errors lead to grave life-threatening consequences such as vascular disease and tumor metastasis. Understanding the signaling mechanisms and driving factors of this process will be important to prevent such mishaps and treat the disorders that arise from erroneous division and migration.

Migration is a dynamic process that is spatially and temporally regulated. The migrating cell is a polarized entity thought to possess a segregated front end and rear end. Rac or Cdc42 localization at the leading edge serves as a signal for actin polymerization at the lamellipodia. Other molecules that regulate formation of new actin filaments such as PIP2, Arp 2/3, WASP etc also localize to the leading edge (Schaks et al., 2019). The coordinated protrusion of the leading edge, formation of adhesions that attach that edge to ECM, contraction to push the cell body

forward and release of the trailing edge are the key visible steps in slow-migrating cells such as fibroblasts. Each of these spatially distinct processes require specific biochemical signals for initiation and progression (Lauffenburger and Horwitz, 1996).

Given the complexity of this process, several proteins with a wide range of other functions participate in coordinating and regulating the steps in cell migration. Kinases serve to phosphorylate substrates to activate or repress their expression. A prototypic example is protein kinase A (PKA), historically recognized as the key effector of the cyclic-AMP second messenger signaling cascade (Carr et al., 1991; Howe et al., 2005; Krebs et al., 1985). Cyclic AMP is a second messenger that activates this kinase to mediate specific cellular functions. PKA is very promiscuous with targets in the membrane, cytoplasm, nucleus, primary cilia, and mitochondria. Accordingly, PKA targets microtubules, actin and intermediate filaments and forms an integral part of cytoskeletal regulation (Howe, 2004). Specifically, PKA activity in cell migration has been supported by several articles that suggest that inhibition of kinase activity blocks cell migration in a variety of different cell types.

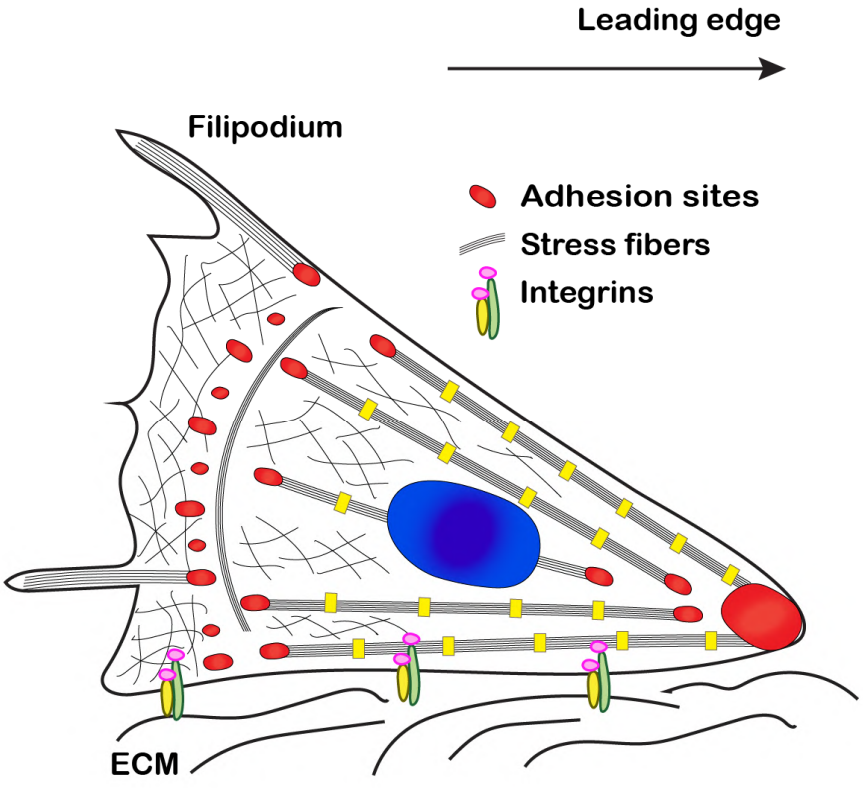

Fig 1: A migrating cell depicting the leading edge and localized proteins

Cell-cell adhesion

The protrusion at the leading edge is further stabilized by adhesion complexes through interaction with actin filaments and signaling to Rho GTPases. Interestingly, adhesion complexes serve to activate and inhibit migration. The smaller Rac-induced adhesions promote quick migration, whereas larger complexes stabilize the cell-ECM contacts and inhibit rear-end dislodging, thereby preventing movement (Lawson and Burridge, 2014).

In the complex extracellular environment filled with chemical and mechanical stimuli, cells require a well-established system of receptors to initiate cell-cell contact. Cells adhere to each other and to the extracellular matrix via cell adhesion molecules (CAMs). Cadherins and integrins are two classes of best-studied cell-adhesion receptors. While these two receptors are placed under the same category, they perform different functions. Integrins enable cell contact with the extracellular matrix and cadherins initiate contact between two or more cells with each other (Parsons et al., 2010). Understanding what drives or interrupts the contact between cell adhesion molecules and actin cytoskeleton is an area of immense research. Focal adhesion molecules enable interaction between integrins and actin. Cadherins interact with the actin cytoskeleton through the catenin family of proteins such as alpha, beta and p120 catenin.

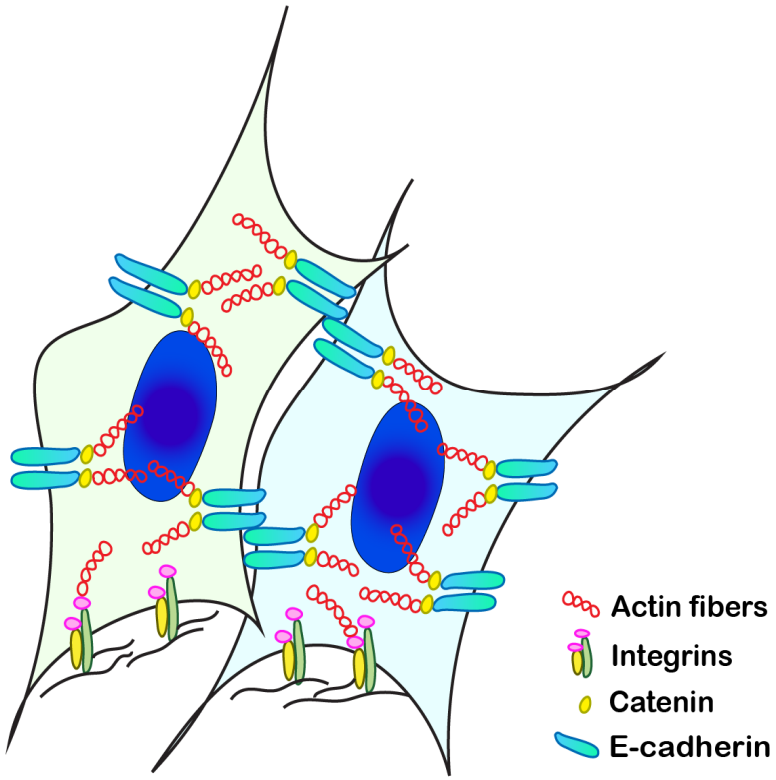

Fig 2: Cell-cell adhesion contacts depicted between two cells

AKAP-mediated signaling in cell migration and cell-cell adhesion

A-kinase anchoring proteins (AKAPs) spatially target kinases and phosphatases to specific cellular locations at a given time (Logue and Scott, 2010). Accordingly, they are important elements in the control of signaling events that drive cell migration and adhesion. Several AKAPs have been studied in this context. Particularly, AKAP79/150 has been found to form complexes with cadherin and beta catenin in neurons and epithelial cells (Gorski et al., 2005).

AKAP220 has been found to participate in mobilizing a microtubule-associated network in the leading edge of cells by integrating cAMP and calcium signals. This delineates the leading edge

from trailing edge, a prerequisite for cell migration (Logue et al., 2011). IQGAP1 controls cell morphology and mobility by binding to actin, calmodulin, cadherin, Rac, Rho A, Cdc42 etc. Further, this GTPase activating protein also affects microtubule dynamics in migrating cells through interaction with microtubule plus-end tracking proteins (+TIPs), CLIP-170, and CLASP2. AKAP220 binds and targets IQGAP1 to specific locations and is responsible for its spatial and temporal activity. Thus, this scaffolding protein plays an indirect role in all the processes controlled by IQGAP1 (Logue et al., 2011).

RESULTS

AKAP220 positions kinases and phosphatases that drive cell proliferation

AKAP220 has been shown to suppress GSK3β to enable recruitment of plus-end microtubule tracking protein CLASP2 (Logue et al., 2011). Further, silencing of AKAP220 affects the rate of microtubule polymerization and eventually, cell migration. We wanted to ask if this is a consequence of slower cell proliferation. Scaffolding proteins contribute to cell division by localizing proteins that regulate the cell cycle. CRISPR-Cas 9 ablation of AKAP220 in mIMCD3 cells led to slower proliferation of these cells as compared to the wildtype (green line, Fig 1). This phenotype was also recapitulated in CRISPR-edited cells that had a form of AKAP220 that does not localize PP1 (blue line, Fig 1). Further, these two mutant cells also showed poor migration compared to the wildtype.

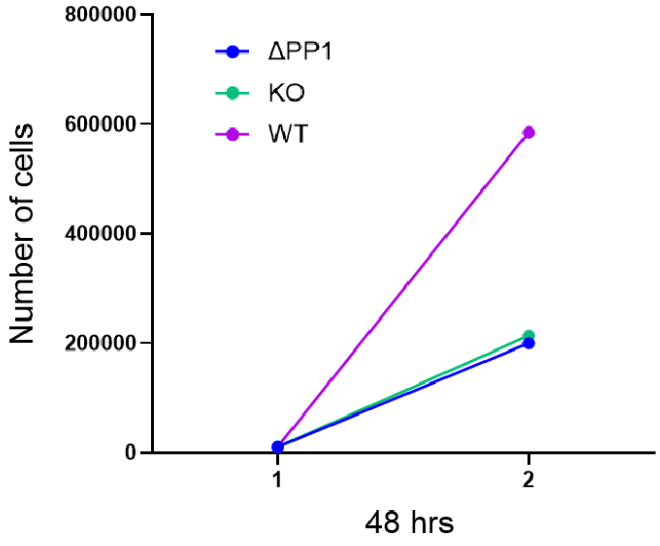

Figure 1: Cell proliferation assay performed over the course of 48 hrs in wildtype (purple), AKAP220KO (green) and AKAP220-ΔPP1 (blue) mIMCD3 cells. The starting cell density was 10,000 cells/well and the final cell density was measured by tryphan blue cell counting assay.

AKAP220 checks excessive cell spreading and enhanced cell-cell contact

Cell spreading is a process where rounded cultured cells flatten and spread out on a substratum. Although both cell movement and spreading require contacts to be made with the substrate, both process are quite different in terms of the energy involved. While cell motility is an active process, adhesion and cell spreading is more passive (McGrath, 2007). However, both process require actin polymerization and myosin contraction. Since AKAP220 is an important contributor to actin dynamics, we asked if this scaffold is also important for cell spreading and cell-cell contact formation. Upon culturing, mIMCD3 cells that lack AKAP220 spread more and form more cell-cell contacts as compared to wildtype. Further, this phenotype is also recapitulated in mutant AKAP220-ΔPP1 cells, potentially implicating PP1 as an important factor in actin polymerization, cellular tension and cell-cell contact formation.

Immunofluorescence experiments were performed with E-cadherin (green), actin (red) and DAPI (blue) (Fig 2A-C). These representative images show that AKAP220KO and AKAP220-ΔPP1 cells spread more than the wildtype when plated at the same cell density, substrate and time (Fig 2A-F). The quantification for total cell area is presented from three independent experiments (Fig 2G).Further, a close look at E-cadherin and actin staining also shows that the mutant cells contact each other extensively compared to the wildtype. In contrast, the wildtype cells have more apparent lamellipodia and fewer points of contact with neighboring cells. This led us to ask if cell adhesion molecules are affected by the loss of this scaffolding protein, AKAP220.

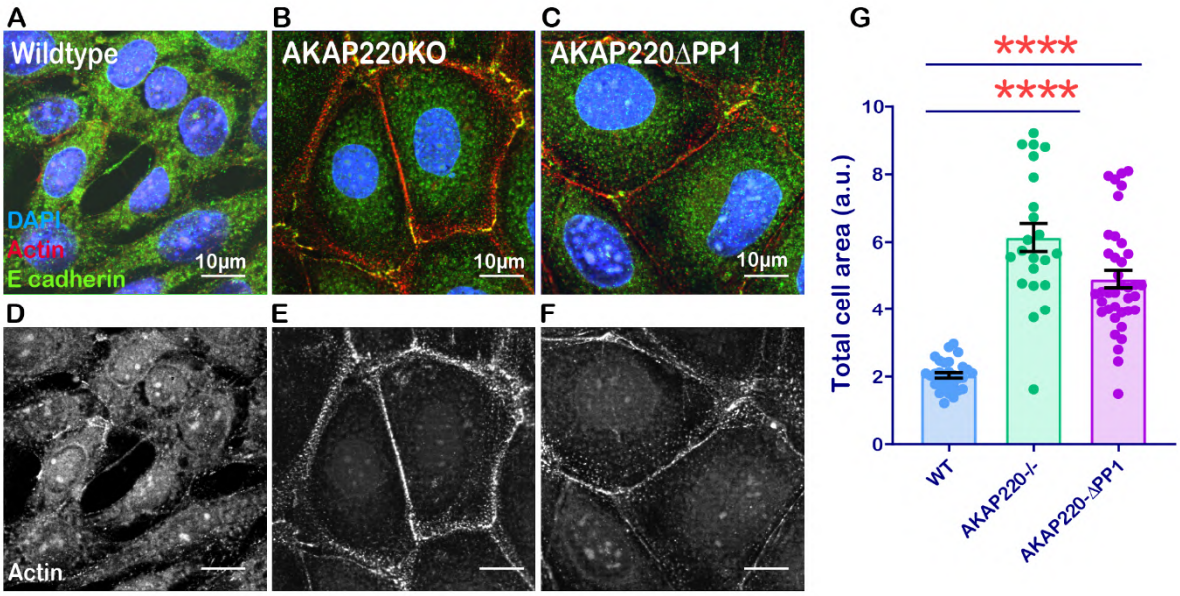

Figure 2: AKAP220 checks excessive cell spreading and enhanced cell-cell contact

A-C) Immunofluorescence staining of E-cadherin (green), actin (red) and DAPI (blue) was performed in wildtype, AKAP220KO and AKAP220- ΔPP1 mIMCD3 cells. **D-F)** Grey scale images of Actin staining show individual cell area. It also delineates increased colocalization with E-cadherin at cell-cell junctions of mutant cells. Cell spreading was evaluated by measuring the area of each cell using imageJ software. **G)** Quantification shows total cell area from three independent experiments in wildtype (blue), AKAP220KO (green) and AKAP220- ΔPP1 (purple). Scale bars (10μm).

Loss of AKAP220 causes upregulation of cell adhesion molecules

By virtue of its interaction with small GTPase effector protein, IQGAP1, AKAP220 influences cell migration (Logue et al., 2011). Although this could translate into changes in cell adhesion and morphology, this area has not been previously well-studied. Further investigation in wildtype and

AKAP220KO mIMCD3 cell lines led to this robust finding that deletion of this anchoring protein correlated with an enhanced level of several cell adhesion proteins. Specifically, cell-cell adhesion marker E-cadherin is upregulated in AKAP220KO cells compared to wildtype controls. Immunofluorescence images of E-cadherin (green) and DAPI (blue) are presented (Fig 3A-D). The second line of investigation was western blots performed in cell lysates from wildtype and AKAP220KO mIMCD3 cells. The blots recapitulated the upregulation of E-cadherin in AKAP220KO cells compared to wildtype controls (Fig 3E). AKAP220 silencing experiments using siRNA in wildtype mIMCD3 cells recapitulated the upregulation of e-cadherin seen in AKAP220KO cells (Fig 3F). This allowed us to attribute this phenotype to the loss of AKAP220.

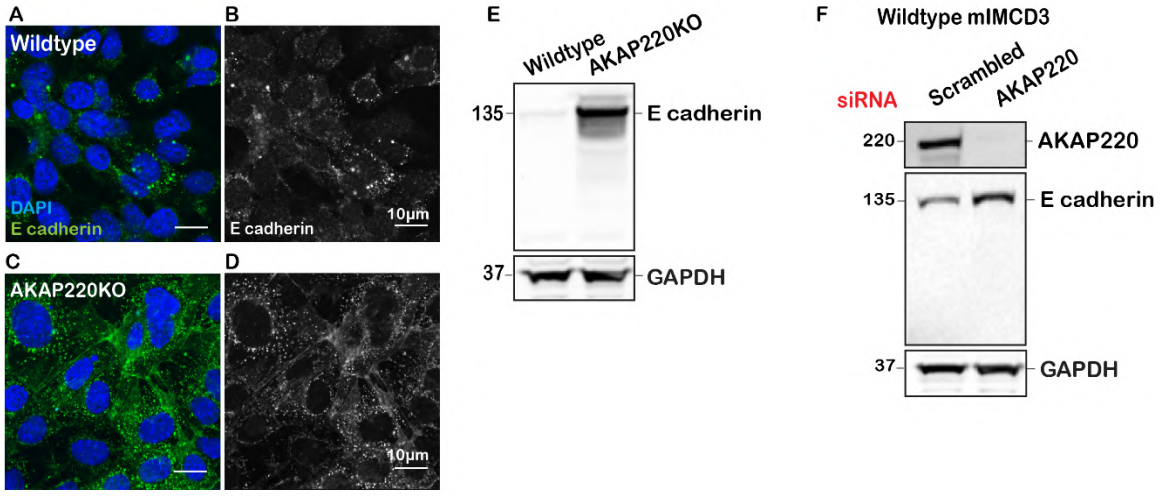

Figure 3: Loss of AKAP220 results in elevated E-cadherin levels.

A-D) Immunofluorescence staining of E-cadherin (green) and DAPI (blue) was performed in **A)** wildtype and **C)** AKAP220KO mIMCD3 cells. **B&D)** Grey scale images show that E-cadherin is upregulated in AKAP220KO compared to wildtype cells. **E)** Immunoblot detection of E-cadherin (top) and GAPDH loading control (bottom), in wildtype (lane 1) and AKAP220KO (lane 2) cell lysates. **F)** Gene silencing of AKAP220 by siRNA treatment. Immunoblot detection of E-cadherin (top) and GAPDH loading control (bottom), in scrambled siRNA (lane 1) and AKAP220 siRNA treated (lane 2) cell lysates. Scale bars (10μm).

Cell-cell junctions are important to maintain epithelial integrity of the cell. The E-cadherin/β-catenin complex has been implicated in this process and aberrant expression of these proteins has been reported to cause malignancies that result from epithelial-mesenchymal transition (Tian et al., 2011) . We investigated β-catenin levels and found that this protein is also elevated in the absence of AKAP220 (Fig 4A-D). Immunofluorescence and western blots show the upregulation of β-catenin (green) in AKAP220KO cells as compared to wildtype (Fig 4E).

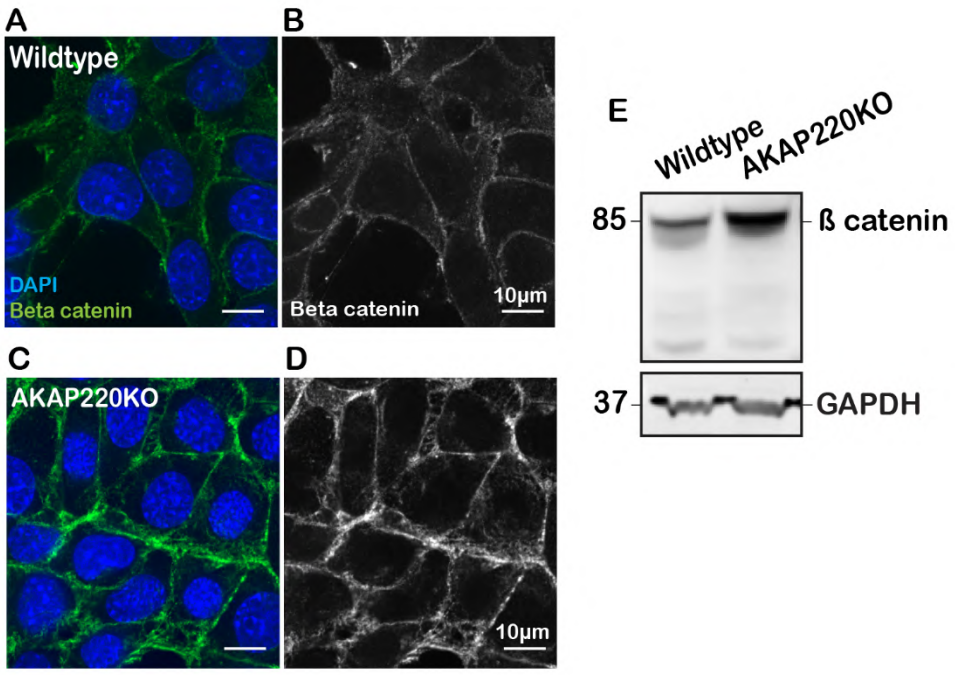

Figure 4: Loss of AKAP220 results in elevated β-catenin levels.

A-D) Immunofluorescence staining of β-catenin (green) and DAPI (blue) was performed in **A)** wildtype and **C)** AKAP220KO mIMCD3 cells. **B&D)** Grey scale images show that β-catenin is upregulated in AKAP220KO compared to wildtype cells. **E)** Immunoblot detection of β-catenin (top) and GAPDH loading control (bottom), in wildtype (lane 1) and AKAP220KO (lane 2) cell lysates. Scale bars (10μm).

The cell-matrix adhesion protein β4 integrin was also elevated by more than two-fold in AKAP220KO compared to wildtype cells (Fig 5A-D). Similar lines of evaluation such as immunofluorescence and western blots (Fig 5E) gave reproducible results.

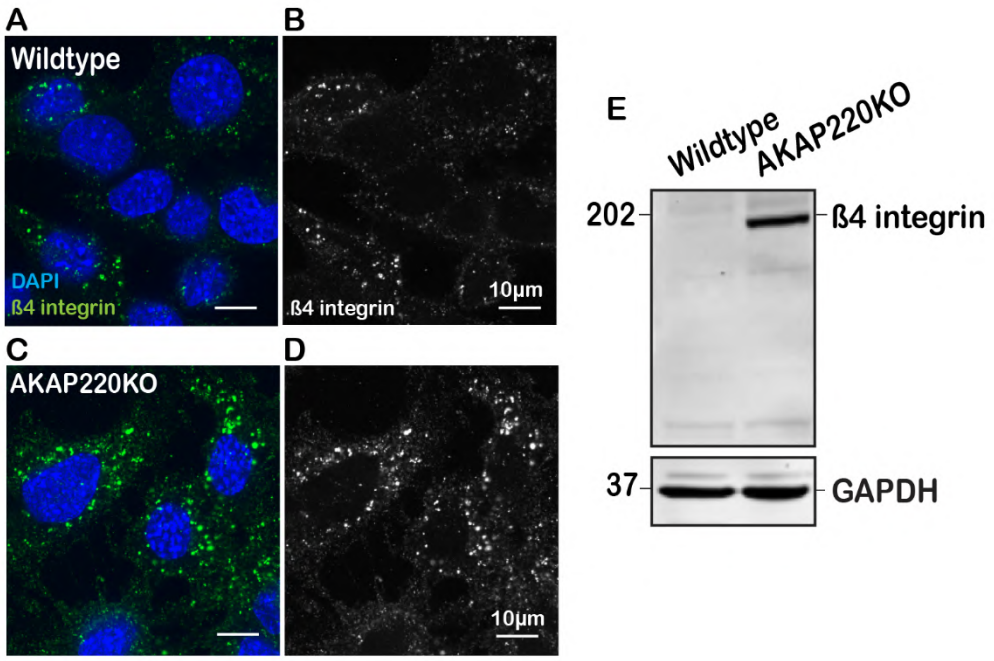

Figure 5: Loss of AKAP220 results in elevated β4 integrin levels.

A-D) Immunofluorescence staining of β4 integrin (green) and DAPI (blue) was performed in **A)** wildtype and **C)** AKAP220KO mIMCD3 cells. **B&D)** Grey scale images show that β4 integrin is upregulated in AKAP220KO compared to wildtype cells. **E)** Immunoblot detection of β4 integrin (top) and GAPDH loading control (bottom), in wildtype (lane 1) and AKAP220KO (lane 2) cell lysates.

Actin dynamics contributes to synthesis of cell adhesion molecules

The Rho small GTPase family comprised of Rho, Rac and Cdc42 regulate assembly, morphology, and maturation of cell-cell junctions (Lawson and Burridge, 2014). AKAP220 also interacts with the Rho-family GTPase effector protein IQGAP1 near the cell cortex to positively regulate actin polymerization (Logue et al., 2011). We found in some of our recent studies that disruption of AKAP220-signaling impacts the distribution and dynamics of actin filaments (chapter 3). This led us to ask if manipulating actin filaments in mIMCD3 cells affects E-cadherin synthesis or localization.

Interestingly, recapitulating actin filament breakdown and poor polymerization seen in AKAP220KO cells by manipulating wildtype mIMCD3 upregulated E-cadherin in these cells (Fig 6A-F). We used cytochalasin D as a tool to pharmacologically target wildtype mIMCD3 cells. Both the cell adhesion molecules are impacted by poor actin filament polymerization in wildtype mIMCD3 cells (Fig 6G). When AKAP220KO cells are treated with cytochalasin D, E-cadherin is elevated even more (Fig 6H-M). But surprisingly, this manipulation of the AKAP220 null cells does not result in further elevation of β4 integrin (Fig 6N). Instead, it results in reduction or maintenance of this protein based on the dose of cytochalasin D used. Since there is a drug-induced elevation of β4 integrin in wildtype cells but not AKAP220KO cells, it is possible that beyond a certain threshold, further actin filament breakdown does not influence this specific integrin.

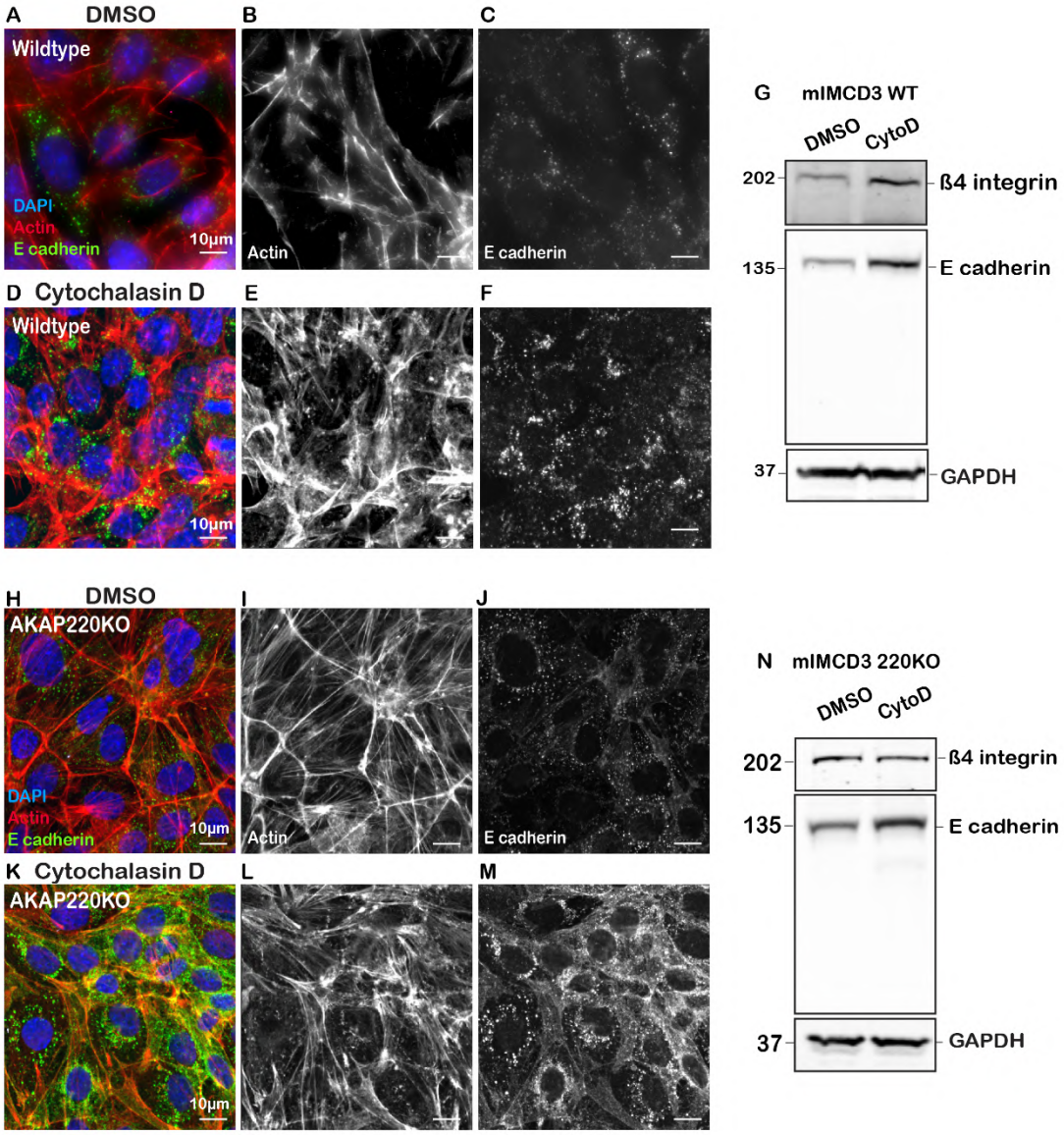

Figure 6: Cytochalasin-D treatment affects expression of CAMs.

Cytochalasin D depolymerizes actin barriers. **A-F**) Immunofluorescent detection of actin (red), E-cadherin (green) and DAPI (blue) in wildtype mIMCD3 cells treated with **A**) DMSO or **D**) 200nM Cytochalasin D. Grey scale images of actin in **B)** DMSO or **E**) 200nM Cytochalasin D treated cells emphasize drug-induced changes in actin cytoskeleton. Grey scale images of E-cadherin in **C)** DMSO or **F**) 200nM Cytochalasin D treated cells emphasize drug-induced

changes in E-cadherin expression. **G)** Immunoblot detection of β4 integrin (top), E-cadherin (mid) and GAPDH loading control (bottom), in DMSO (lane 1) and Cytochalasin D-treated (lane 2) cell lysates. **H-M**) Immunofluorescent detection of actin (red), E-cadherin (green) and DAPI (blue) in AKAP220KO mIMCD3 cells treated with **H**) DMSO or **K**) 200nM Cytochalasin D. Grey scale images of actin in **I)** DMSO or **L**) 200nM Cytochalasin D treated cells emphasize drug-induced changes in actin cytoskeleton. Grey scale images of E-cadherin in **J)** DMSO or **M**) 200nM Cytochalasin D treated cells emphasize drug-induced changes in E-cadherin expression. **N)** Immunoblot detection of β4 integrin (top), E-cadherin (mid) and GAPDH loading control (bottom), in DMSO (lane 1) and Cytochalasin D-treated (lane 2) cell lysates. Scale bars (10μm).

Diverse effect of actin modulating drugs on CAM proteins

Stabilizing actin polymerization affects distribution but not the level of E-cadherin in AKAP220KO mIMCD3 cells (Fig 7). Jasplakinolide is a macrocyclic peptide that stabilizes f-actin and augments the formation of actin barriers (Holzinger, 2009). Drug treatment (500nM) for 1.5 h rescues β4 integrin levels to baseline, but not E-cadherin (Fig 7I). It is possible there is a dose-dependent effect of actin modulating drugs on different CAM proteins.

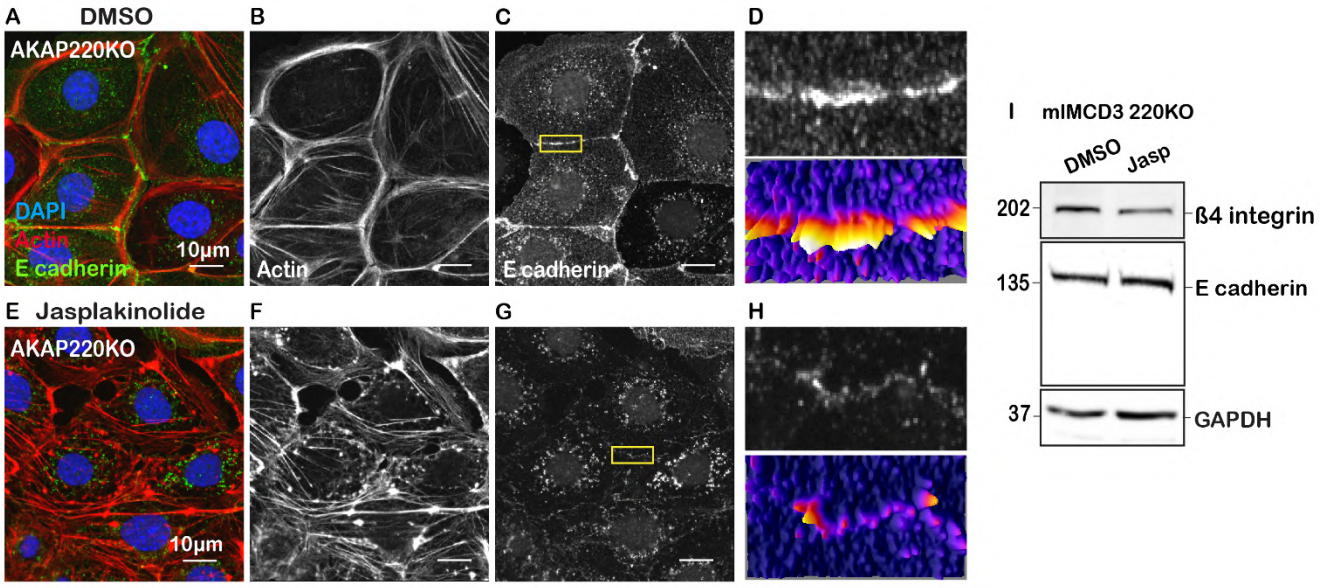

Figure 7: Jasplakinolide treatment affects expression of CAMs.

Jasplakinolide stabilizes actin barriers. **A-F**) Immunofluorescent detection of actin (red), E-cadherin (green) and DAPI (blue) in wildtype mIMCD3 cells treated with **A**) DMSO or **E**) 500nM Jasplakinolide. Grey scale images of actin in **B)** DMSO or **F**) Jasplakinolide treated cells emphasize drug-induced changes in actin cytoskeleton. Grey scale images of E-cadherin in **C)** DMSO or **G**) Jasplakinolide treated cells emphasize drug-induced changes in E-cadherin expression. Enlarged regions of E-cadherin (top) and their corresponding 3D surface plots

(bottom) in **D)** DMSO or **H)** Jasplakinolide treated cells represent distribution and intensity of E-cadherin in cell-cell junctions. **I)** Immunoblot detection of β4 integrin (top), E-cadherin (mid) and GAPDH loading control (bottom), in DMSO (lane 1) and Jasplakinolide-treated (lane 2) AKAP220KO mIMCD3 cell lysates. Scale bars (10μm).

Focal adhesions are enhanced in AKAP220-null cells

Focal adhesions link integrins to the actin cytoskeleton on the inside of cells and extracellular matrix on the outside. The smaller focal complexes are regulated by Rac and Cdc42, while the larger ones are Rho-signaling dependent (Burridge, 2017). As AKAP220 interacts with the Rho-GTPase effector protein IQGAP1, this anchoring protein positively regulates several cytoskeletal elements such as actin and microtubules. By extension, we now find that AKAP220 also plays an important role in cell-cell contact as well as cell-matrix interaction by modulating localization and expression of cell adhesion molecules. As a further line of investigation, we stained for paxillin in the three mIMCD3 cell lines to visualize focal adhesions in these cells.

Immunofluorescence experiments show that the mutant AKAP220KO and AKAP220-ΔPP1 cells have significantly larger focal adhesions (Fig 8A-F). 3D surface plots reveal longer and more continuous paxillin staining in the focal adhesions of mutant cells as compared to wildtype (Fig 8I & L). The latter have more fractured and less evenly distributed paxillin staining. Interestingly, there is no difference in total paxillin level between the cell types (Fig 8M).

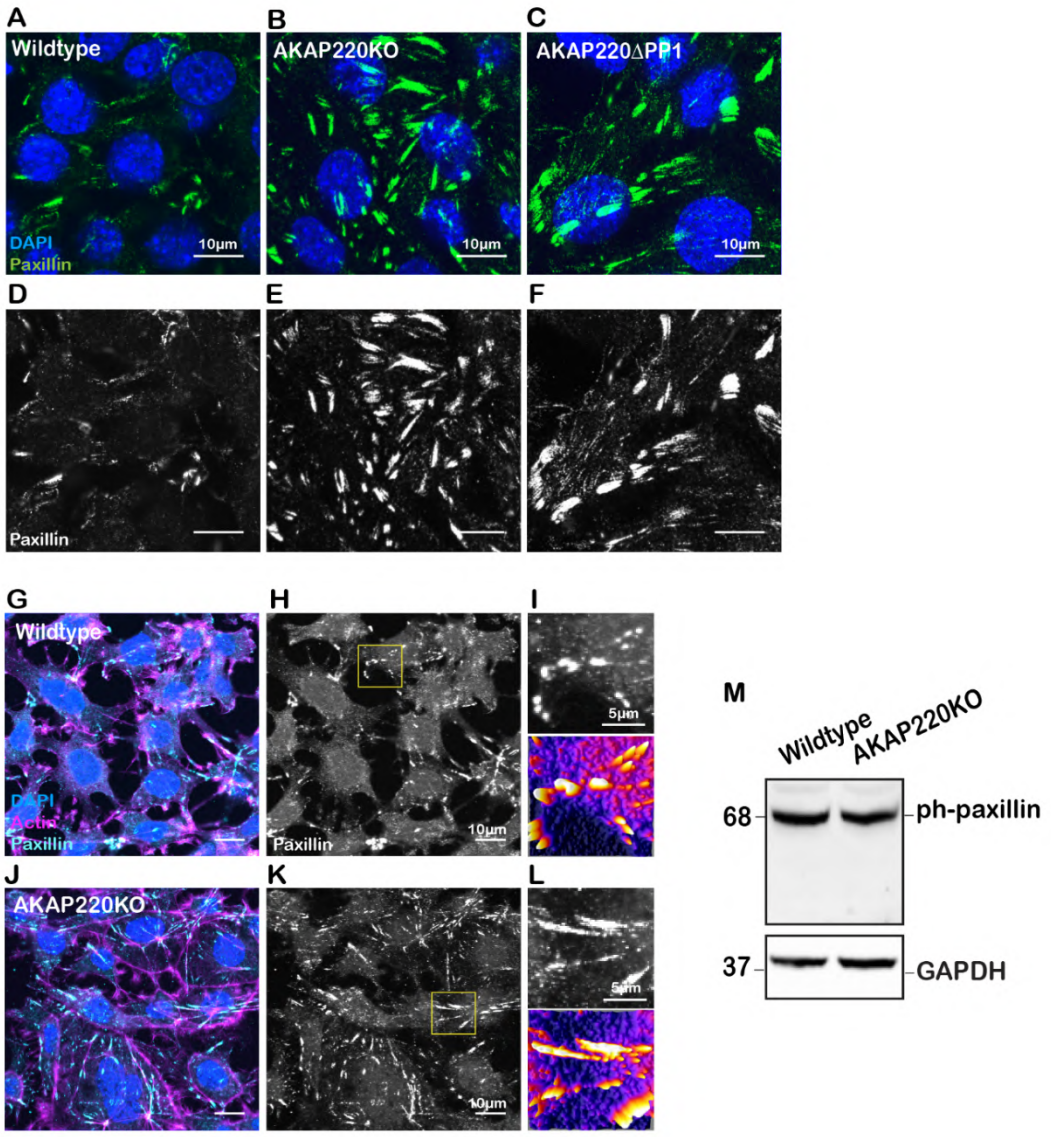

Figure 8: Loss of AKAP220 enhances focal adhesion complexes.

A-F) Immunofluorescence staining of paxillin (green) and DAPI (blue) was performed in **A)** wildtype, **B)** AKAP220KO and **C)** AKAP220-ΔPP1 mIMCD3 cells. **D-F)** Grey scale images of paxillin show that focal adhesions are larger in the mutant cells compared to wildtype cells. **G-L)** Lower magnification images of wildtype and AKAP220KO cells. Immunofluorescence staining of paxillin (cyan), actin (magenta) and DAPI (blue) was performed in **G)** wildtype and **J)** AKAP220KO mIMCD3 cells. Grey scale images of paxillin in **H)** wildtype and **K)** AKAP220KO

mIMCD3 cells show that the distribution of focal adhesions is uniform between the cell types. Enlarged regions of paxillin (top) and their corresponding 3D surface plots (bottom) in **I)** wildtype and **L)** AKAP220KO mIMCD3 cells represent distribution and intensity paxillin in focal adhesion complexes. **M)** Immunoblot detection of ph-paxillin (top) and GAPDH loading control (bottom), in wildtype (lane 1) and AKAP220KO (lane 2) cell lysates. Scale bars (10μm).

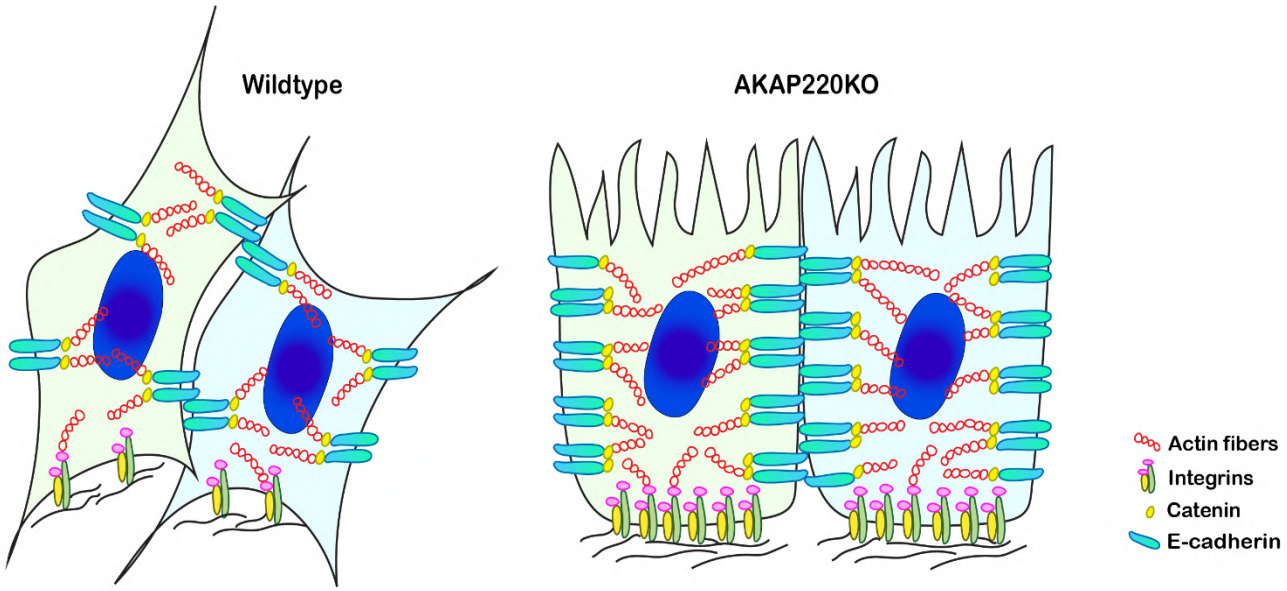

Figure 9: Proposed model of cell adhesion.

Wildtype cells show fewer cell-cell and cell-matrix adhesion protens, evenly formed lamellipodia and fewer contacts with the adjacent cell. AKAP220KO cells depict the upregulation of cell-cell and cell-matrix adhesion proteins, flattened morphology and more spread out sticky cells forming more contacts with each other and the matrix.

Materials and methods

Cell culture

mIMCD3 cells were maintained in DMEM: F12 1:1 media supplemented with 10% FBS and penicillin/streptomycin. Cells were transfected with plasmids using Mirus TransIT-LT1 transfection reagent and incubated for 48-72 hrs before lysis or fixation. All cell lines were maintained in a 5% CO2 incubator at 37 °C.

Immunoblotting and blot analysis

Cells were grown to the desired confluence and washed once with PBS at room temperature. Cold lysis buffer (20 mM HEPES, (pH 7.4),150 mM NaCl,1 mM EDTA,1% triton X-100 in water) was added along with protease and phosphatase inhibitors and the plate was rocked gently at 4 degrees for 10 mins. The cell lysate was then scarped into a pre-chilled tube and cleared at 12,000*g for 10 min at 4 degrees. A BCA assay (Pierce) was used to determine protein concentrations, and 30µg of protein was loaded onto a Bolt 4–12% bis-Tris gel (Life Technologies). The cleared lysate was boiled in 2X SDS loading buffer for 10 min before loading. Proteins were transferred to nitrocellulose membrane and blocked in 5% milk. The blot was incubated in primary antibody at 1:1000 or as specified by the manufacturer overnight at 4 °C. Immunoblots were washed (3 times, 10 mins each) in TBST before incubation in a 1:10,000 secondary antibody for 1 hr at room temperature. Immunoblots were washed again in TBST (3 times, 10 mins each) before imaging on an iBright FL1000 (Thermo Fisher Scientific) with Super Signal Dura ECL reagent (Thermo Fisher Scientific). Densitometry for blot quantification was done using thermo fisher's software.

Immunofluorescence and microscopy

Sample preparation: Cells were seeded on acid-washed coverslips in 12-well plates. After they achieve the desired confluence, the wells were rinsed thrice with PBS and fixed with 4% paraformaldehyde in PBS or 10% ice cold methanol (based on the antibody specification) for 12 mins. After fixation, the cells were permeabilized in PBS+0.1%Triton x-100+1%BSA for 12 mins, blocked with 2%BSA for 30 mins and treated with the respective primary antibodies overnight. After thorough washing in PBS the next day (3 times, 5mins each), secondary antibodies conjugated to Alexa fluor dyes were added for 2 hours. After 2 washes in PBS, DAPI along with or without the actin probe (based on the experiment) was added for 10 mins. The coverslips were washed 2 more times in PBS and mounted on slides using ProLong Diamond Antifade Mountant (Life Technologies).

Imaging and analysis: Cells were imaged on a Keyence BZ-X710 microscope (Keyence, Itasca, IL) using the relevant filter cubes for DAPI (blue filter), Actin (red filter), Cortactin (green filter). All images were acquired with the same magnification (100X, oil immersion), exposure time, and illumination intensity. Images were quantified and processed using ImageJ software.

Antibodies

The following antibodies were used in this study for immunoblotting: AKAP220 (custom rabbit polyclonal,1:1000), GAPDH (Novus, mouse monoclonal, 1:5000), E-cadherin (Thermo Fisher # BDB610181, 1:1000), Beta catenin (BD transduction # 610154, 1:1000) and Actin (Molecular probe, R37112, 1drop/ml).

Statistics for all experiments

Statistical analysis was performed using an unpaired two-tailed Student's t-test or one-way ANOVA (based on the number of samples) in GraphPad Prism software. All values are reported as mean ± standard error of the mean (s.e.m) with p-values less than 0.05 considered statistically significant. For each experiment, number of independent experiments (N) and number of individual points from all experiments (n) are presented.

Cell area in ImageJ

For measuring cell area, lines were drawn to enclose each cell and the area was generated using ImageJ. Amalgamated data from three experiments are presented.

Drug treatment experiments

mIMCD3 cells were seeded on cover slips in 12-well plates and allowed to grow to the desired confluence. They were treated with, 200nM cytochalasin D for 4 hours or 500nM Jasplakinolide for 1.5 hours and fixed immediately after treatment (as previously described). The cells were stained for one of the several proteins investigated in our study and DAPI to mark DNA.

References

1. Badano, J.L., Mitsuma, N., Beales, P.L., and Katsanis, N. (2006). The Ciliopathies: An Emerging Class of Human Genetic Disorders. Annu. Rev. Genomics Hum. Genet. *7*, 125–148.
2. Balliu, M., Guandalini, L., Romanelli, M.N., D'Amico, M., and Paoletti, F. (2015). HDAC-inhibitor (S)-8 disrupts HDAC6-PP1 complex prompting A375 melanoma cell growth arrest and apoptosis. J. Cell. Mol. Med. *19*, 143–154.
3. Bankir, L., Bouby, N., and Ritz, E. (2013). Vasopressin: a novel target for the prevention and retardation of kidney disease? Nat. Rev. Nephrol. *9*, 223–239.
4. Bastos, A.P., and Onuchic, L.F. (2011). Molecular and cellular pathogenesis of autosomal dominant polycystic kidney disease. Braz. J. Med. Biol. Res. Rev. Bras. Pesqui. Medicas E Biol. *44*, 606–617.
5. Biologists, C. of (2007). Actin stage set for ciliogenesis. J. Cell Sci. *120*, e1105–e1105.
6. Blattner, S.M., Hodgin, J.B., Nishio, M., Wylie, S.A., Saha, J., Soofi, A.A., Vining, C., Randolph, A., Herbach, N., Wanke, R., et al. (2013). Divergent functions of the Rho GTPases Rac1 and Cdc42 in podocyte injury. Kidney Int. *84*, 920–930.
7. Bollen, M., Peti, W., Ragusa, M.J., and Beullens, M. (2010). The extended PP1 toolkit: designed to create specificity. Trends Biochem. Sci. *35*, 450–458.
8. Boyault, C., Sadoul, K., Pabion, M., and Khochbin, S. (2007). HDAC6, at the crossroads between cytoskeleton and cell signaling by acetylation and ubiquitination. Oncogene *26*, 5468–5476.
9. Breslow, D.K., Hoogendoorn, S., Kopp, A.R., Morgens, D.W., Vu, B.K., Kennedy, M.C., Han, K., Li, A., Hess, G.T., Bassik, M.C., et al. (2018). A CRISPR-based screen for

Hedgehog signaling provides insights into ciliary function and ciliopathies. Nat. Genet. *50*, 460–471.

10. Brush, M.H., Guardiola, A., Connor, J.H., Yao, T.-P., and Shenolikar, S. (2004). Deactylase inhibitors disrupt cellular complexes containing protein phosphatases and deacetylases. J. Biol. Chem. *279*, 7685–7691.
11. Bucko, P.J., and Scott, J.D. (2021). Drugs that Regulate Local Cell Signaling: AKAP Targeting as a Therapeutic Option. Annu. Rev. Pharmacol. Toxicol. *61*, null.
12. Bucko, P.J., Lombard, C.K., Rathbun, L., Garcia, I., Bhat, A., Wordeman, L., Smith, F.D., Maly, D.J., Hehnly, H., and Scott, J.D. (2019). Subcellular drug targeting illuminates local kinase action. ELife *8*, e52220.
13. Bucko, P.J., Garcia, I., Manocha, R., Bhat, A., Wordeman, L., and Scott, J.D. (2020). Gravin-associated kinase signaling networks coordinate γ-tubulin organization at mitotic spindle poles. J. Biol. Chem. jbc.RA120.014791.
14. Burridge, K. (2017). Focal adhesions: a personal perspective on a half century of progress. FEBS J. *284*, 3355–3361.
15. Carr, D.W., Stofko-Hahn, R.E., Fraser, I.D., Bishop, S.M., Acott, T.S., Brennan, R.G., and Scott, J.D. (1991). Interaction of the regulatory subunit (RII) of cAMP-dependent protein kinase with RII-anchoring proteins occurs through an amphipathic helix binding motif. J. Biol. Chem. *266*, 14188–14192.
16. Casella, J.F., Flanagan, M.D., and Lin, S. (1981). Cytochalasin D inhibits actin polymerization and induces depolymerization of actin filaments formed during platelet shape change. Nature *293*, 302–305.

17. Choi, Y.-H., Suzuki, A., Hajarnis, S., Ma, Z., Chapin, H.C., Caplan, M.J., Pontoglio, M., Somlo, S., and Igarashi, P. (2011). Polycystin-2 and phosphodiesterase 4C are components of a ciliary A-kinase anchoring protein complex that is disrupted in cystic kidney diseases. Proc. Natl. Acad. Sci. *108*, 10679–10684.
18. Copeland, S.J., McRae, A., Guarguaglini, G., Trinkle-Mulcahy, L., and Copeland, J.W. (2018). Actin-dependent regulation of cilia length by the inverted formin FHDC1. Mol. Biol. Cell *29*, 1611–1627.
19. de Diego, A.S., Alonso Guerrero, A., Martínez-A, C., and van Wely, K.H.M. (2014). Dido3-dependent HDAC6 targeting controls cilium size. Nat. Commun. *5*, 3500.
20. Dong, J., Zheng, N., Wang, X., Tang, C., Yan, P., Zhou, H.-B., and Huang, J. (2018). A novel HDAC6 inhibitor exerts an anti-cancer effect by triggering cell cycle arrest and apoptosis in gastric cancer. Eur. J. Pharmacol. *828*, 67–79.
21. Drummond, M.L., Li, M., Tarapore, E., Nguyen, T.T.L., Barouni, B.J., Cruz, S., Tan, K.C., Oro, A.E., and Atwood, S.X. (2018). Actin polymerization controls cilia-mediated signaling. J. Cell Biol. *217*, 3255–3266.
22. Farina, F., Gaillard, J., Guérin, C., Couté, Y., Sillibourne, J., Blanchoin, L., and Théry, M. (2016). The centrosome is an actin-organizing centre. Nat. Cell Biol. *18*, 65–75.
23. Fliegauf, M., Benzing, T., and Omran, H. (2007). When cilia go bad: cilia defects and ciliopathies. Nat. Rev. Mol. Cell Biol. *8*, 880–893.
24. Frame, S., Cohen, P., and Biondi, R.M. (2001). A common phosphate binding site explains the unique substrate specificity of GSK3 and its inactivation by phosphorylation. Mol. Cell *7*, 1321–1327.

25. Freedman, B.S., Lam, A.Q., Sundsbak, J.L., Iatrino, R., Su, X., Koon, S.J., Wu, M., Daheron, L., Harris, P.C., Zhou, J., et al. (2013). Reduced ciliary polycystin-2 in induced pluripotent stem cells from polycystic kidney disease patients with PKD1 mutations. J. Am. Soc. Nephrol. JASN *24*, 1571–1586.

26. Freedman, B.S., Brooks, C.R., Lam, A.Q., Fu, H., Morizane, R., Agrawal, V., Saad, A.F., Li, M.K., Hughes, M.R., Werff, R.V., et al. (2015). Modelling kidney disease with CRISPR-mutant kidney organoids derived from human pluripotent epiblast spheroids. Nat. Commun. *6*, 8715.

27. Giles, R.H., Ajzenberg, H., and Jackson, P.K. (2014). 3D spheroid model of mIMCD3 cells for studying ciliopathies and renal epithelial disorders. Nat. Protoc. *9*, 2725–2731.

28. Goetz, S.C., and Anderson, K.V. (2010). The primary cilium: a signalling centre during vertebrate development. Nat. Rev. Genet. *11*, 331–344.

29. Gorski, J.A., Gomez, L.L., Scott, J.D., and Dell'Acqua, M.L. (2005). Association of an A-Kinase-anchoring Protein Signaling Scaffold with Cadherin Adhesion Molecules in Neurons and Epithelial Cells. Mol. Biol. Cell *16*, 3574–3590.

30. Haggarty, S.J., Koeller, K.M., Wong, J.C., Grozinger, C.M., and Schreiber, S.L. (2003). Domain-selective small-molecule inhibitor of histone deacetylase 6 (HDAC6)-mediated tubulin deacetylation. Proc. Natl. Acad. Sci. U. S. A. *100*, 4389–4394.

31. Halvorson, C.R., Bremmer, M.S., and Jacobs, S.C. (2010). Polycystic kidney disease: inheritance, pathophysiology, prognosis, and treatment. Int. J. Nephrol. Renov. Dis. *3*, 69–83.

32. Harris, P.C., and Torres, V.E. (2014). Genetic mechanisms and signaling pathways in autosomal dominant polycystic kidney disease. J. Clin. Invest. *124*, 2315–2324.

33. Hemmelgarn, B.R., Zhang, J., Manns, B.J., Tonelli, M., Larsen, E., Ghali, W.A., Southern, D.A., McLaughlin, K., Mortis, G., and Culleton, B.F. (2006). Progression of kidney dysfunction in the community-dwelling elderly. Kidney Int. *69*, 2155–2161.

34. Holzinger, A. (2009). Jasplakinolide: an actin-specific reagent that promotes actin polymerization. Methods Mol. Biol. Clifton NJ *586*, 71–87.

35. Hoshi, N., Langeberg, L.K., and Scott, J.D. (2005). Distinct enzyme combinations in AKAP signalling complexes permit functional diversity. Nat. Cell Biol. *7*, 1066–1073.

36. Howe, A.K. (2004). Regulation of actin-based cell migration by cAMP/PKA. Biochim. Biophys. Acta *1692*, 159–174.

37. Howe, A.K., Baldor, L.C., and Hogan, B.P. (2005). Spatial regulation of the cAMP-dependent protein kinase during chemotactic cell migration. Proc. Natl. Acad. Sci. *102*, 14320–14325.

38. Hubbert, C., Guardiola, A., Shao, R., Kawaguchi, Y., Ito, A., Nixon, A., Yoshida, M., Wang, X.-F., and Yao, T.-P. (2002). HDAC6 is a microtubule-associated deacetylase. Nature *417*, 455–458.

39. Hughes, J., Ward, C.J., Peral, B., Aspinwall, R., Clark, K., San Millán, J.L., Gamble, V., and Harris, P.C. (1995). The polycystic kidney disease 1 (PKD1) gene encodes a novel protein with multiple cell recognition domains. Nat. Genet. *10*, 151–160.

40. Janke, C., and Magiera, M.M. (2020). The tubulin code and its role in controlling microtubule properties and functions. Nat. Rev. Mol. Cell Biol. *21*, 307–326.

41. Jo, I., Ward, D.T., Baum, M.A., Scott, J.D., Coghlan, V.M., Hammond, T.G., and Harris, H.W. (2001). AQP2 is a substrate for endogenous PP2B activity within an inner medullary AKAP-signaling complex. Am. J. Physiol.-Ren. Physiol. *281*, F958–F965.

42. Kim, J., Jo, H., Hong, H., Kim, M.H., Kim, J.M., Lee, J.-K., Heo, W.D., and Kim, J. (2015). Actin remodelling factors control ciliogenesis by regulating YAP/TAZ activity and vesicle trafficking. Nat. Commun. *6*, 6781.

43. Klymkowsky, M.W. (1999). Weaving a tangled web: the interconnected cytoskeleton. Nat. Cell Biol. *1*, E121–E123.

44. Krebs, E.G., Blumenthal, D.K., Edelman, A.M., and Hales, C.N. (1985). Role of Cyclic-AMP-Dependent Protein Kinase in the Regulation of Cellular Processes. In Mechanisms of Receptor Regulation, G. Poste, and S.T. Crooke, eds. (Boston, MA: Springer US), pp. 159–195.

45. Langeberg, L.K., and Scott, J.D. (2015). Signalling scaffolds and local organization of cellular behaviour. Nat. Rev. Mol. Cell Biol. *16*, 232–244.

46. Lauffenburger, D.A., and Horwitz, A.F. (1996). Cell Migration: A Physically Integrated Molecular Process. Cell *84*, 359–369.

47. Lawson, C.D., and Burridge, K. (2014). The on-off relationship of Rho and Rac during integrin-mediated adhesion and cell migration. Small GTPases *5*.

48. Lee, K., Battini, L., and Gusella, G.L. (2011). Cilium, centrosome and cell cycle regulation in polycystic kidney disease. Biochim. Biophys. Acta *1812*, 1263–1271.

49. Lester, L.B., Coghlan, V.M., Nauert, B., and Scott, J.D. (1996). Cloning and characterization of a novel A-kinase anchoring protein. AKAP 220, association with testicular peroxisomes. J. Biol. Chem. *271*, 9460–9465.

50. Li, X., Qi, N., Li, L., Wu, M., and Mei, C. (2016). Cytosolic HDAC6 is accumulated in cystic kidneys. Kidney Int. *90*, 705.

51. Logue, J.S., and Scott, J.D. (2010). Organizing signal transduction through A-kinase Anchoring Proteins (AKAPs). FEBS J. *277*, 4370–4375.

52. Logue, J.S., Whiting, J.L., Tunquist, B., Sacks, D.B., Langeberg, L.K., Wordeman, L., and Scott, J.D. (2011). AKAP220 Protein Organizes Signaling Elements That Impact Cell Migration. J. Biol. Chem. *286*, 39269–39281.

53. Long, H., and Huang, K. (2020). Transport of Ciliary Membrane Proteins. Front. Cell Dev. Biol. *7*.

54. Lygren, B., Carlson, C.R., Santamaria, K., Lissandron, V., McSorley, T., Litzenberg, J., Lorenz, D., Wiesner, B., Rosenthal, W., Zaccolo, M., et al. (2007). AKAP complex regulates Ca2+ re-uptake into heart sarcoplasmic reticulum. EMBO Rep. *8*, 1061–1067.

55. Ma, M., Tian, X., Igarashi, P., Pazour, G.J., and Somlo, S. (2013). Loss of cilia suppresses cyst growth in genetic models of autosomal dominant polycystic kidney disease. Nat. Genet. *45*, 1004–1012.

56. Ma, M., Gallagher, A.-R., and Somlo, S. (2017). Ciliary Mechanisms of Cyst Formation in Polycystic Kidney Disease. Cold Spring Harb. Perspect. Biol. *9*.

57. May, E.A., Kalocsay, M., D'Auriac, I.G., Gygi, S.P., Nachury, M.V., and Mick, D.U. (2020). Time-resolved proteomic profiling of the ciliary Hedgehog response reveals that GPR161 and PKA undergo regulated co-exit from cilia. BioRxiv 2020.07.29.225797.

58. McGrath, J.L. (2007). Cell Spreading: The Power to Simplify. Curr. Biol. *17*, R357–R358.

59. Mochizuki, T., Wu, G., Hayashi, T., Xenophontos, S.L., Veldhuisen, B., Saris, J.J., Reynolds, D.M., Cai, Y., Gabow, P.A., Pierides, A., et al. (1996). PKD2, a gene for

polycystic kidney disease that encodes an integral membrane protein. Science *272*, 1339–1342.

60. Mukhopadhyay, S., Wen, X., Ratti, N., Loktev, A., Rangell, L., Scales, S.J., and Jackson, P.K. (2013). The ciliary G-protein-coupled receptor Gpr161 negatively regulates the Sonic hedgehog pathway via cAMP signaling. Cell *152*, 210–223.
61. Noda, Y., Sohara, E., Ohta, E., and Sasaki, S. (2010). Aquaporins in kidney pathophysiology. Nat. Rev. Nephrol. *6*, 168–178.
62. Parnell, S.C., Puri, S., Wallace, D.P., and Calvet, J.P. (2012). Protein Phosphatase-1α Interacts with and Dephosphorylates Polycystin-1. PLoS ONE *7*.
63. Parsons, J.T., Horwitz, A.R., and Schwartz, M.A. (2010). Cell adhesion: integrating cytoskeletal dynamics and cellular tension. Nat. Rev. Mol. Cell Biol. *11*, 633–643.
64. Piccolo, S., Dupont, S., and Cordenonsi, M. (2014). The Biology of YAP/TAZ: Hippo Signaling and Beyond. Physiol. Rev. *94*, 1287–1312.
65. Plotnikova, O.V., Pugacheva, E.N., and Golemis, E.A. (2009). Chapter 7 - Primary Cilia and the Cell Cycle. In Methods in Cell Biology, R.D. Sloboda, ed. (Academic Press), pp. 137–160.
66. Portran, D., Schaedel, L., Xu, Z., Théry, M., and Nachury, M.V. (2017). Tubulin acetylation protects long-lived microtubules against mechanical ageing. Nat. Cell Biol. *19*, 391–398.
67. Ran, J., Yang, Y., Li, D., Liu, M., and Zhou, J. (2015). Deacetylation of α-tubulin and cortactin is required for HDAC6 to trigger ciliary disassembly. Sci. Rep. *5*, 12917.
68. Ran, J., Liu, M., Feng, J., Li, H., Ma, H., Song, T., Cao, Y., Zhou, P., Wu, Y., Yang, Y., et al. (2020). ASK1-Mediated Phosphorylation Blocks HDAC6 Ubiquitination and

Degradation to Drive the Disassembly of Photoreceptor Connecting Cilia. Dev. Cell *53*, 287-299.e5.

69. Saborio, P., Krieg Jr., R.J., Kuemmerle, N.B., Norkus, E.P., Schwartz, C.C., and Chan, J.C.M. (2000). α-Tocopherol modulates lipoprotein cytotoxicity in obstructive nephropathy. Pediatr. Nephrol. *14*, 740–746.
70. Satir, P., Pedersen, L.B., and Christensen, S.T. (2010). The primary cilium at a glance. J. Cell Sci. *123*, 499–503.
71. Schaks, M., Giannone, G., and Rottner, K. (2019). Actin dynamics in cell migration. Essays Biochem. *63*, 483–495.
72. Schillace, R.V., and Scott, J.D. (1999). Association of the type 1 protein phosphatase PP1 with the A-kinase anchoring protein AKAP220. Curr. Biol. CB *9*, 321–324.
73. Schillace, R.V., Voltz, J.W., Sim, A.T., Shenolikar, S., and Scott, J.D. (2001). Multiple interactions within the AKAP220 signaling complex contribute to protein phosphatase 1 regulation. J. Biol. Chem. *276*, 12128–12134.
74. Schnoor, M., Stradal, T.E., and Rottner, K. (2018). Cortactin: Cell Functions of A Multifaceted Actin-Binding Protein. Trends Cell Biol. *28*, 79–98.
75. Scott, J.D., and Pawson, T. (2009). Cell Signaling in Space and Time: Where Proteins Come Together and When They're Apart. Science *326*, 1220–1224.
76. Smith, F.D., Esseltine, J.L., Nygren, P.J., Veesler, D., Byrne, D.P., Vonderach, M., Strashnov, I., Eyers, C.E., Eyers, P.A., Langeberg, L.K., et al. (2017). Local protein kinase A action proceeds through intact holoenzymes. Science *356*, 1288–1293.
77. Smith, F.D., Omar, M.H., Nygren, P.J., Soughayer, J., Hoshi, N., Lau, H.-T., Snyder, C.G., Branon, T.C., Ghosh, D., Langeberg, L.K., et al. (2018). Single nucleotide

polymorphisms alter kinase anchoring and the subcellular targeting of A-kinase anchoring proteins. Proc. Natl. Acad. Sci. *115*, E11465–E11474.

78. Somatilaka, B.N., Hwang, S.-H., Palicharla, V.R., White, K.A., Badgandi, H., Shelton, J.M., and Mukhopadhyay, S. (2020). Ankmy2 Prevents Smoothened-Independent Hyperactivation of the Hedgehog Pathway via Cilia-Regulated Adenylyl Cyclase Signaling. Dev. Cell.
79. Song, H., Niu, X., Quan, J., Li, Y., Yuan, L., Wang, J., Ma, C., and Ma, E. (2020). Discovery of specific HDAC6 inhibitor with anti-metastatic effects in pancreatic cancer cells through virtual screening and biological evaluation. Bioorganic Chem. *97*, 103679.
80. Stefan, E., Aquin, S., Berger, N., Landry, C.R., Nyfeler, B., Bouvier, M., and Michnick, S.W. (2007). Quantification of dynamic protein complexes using Renilla luciferase fragment complementation applied to protein kinase A activities in vivo. Proc. Natl. Acad. Sci. *104*, 16916–16921.
81. Streets, A., and Ong, A. (2020). Post-translational modifications of the polycystin proteins. Cell. Signal. *72*, 109644.
82. Streets, A.J., Wessely, O., Peters, D.J.M., and Ong, A.C.M. (2013). Hyperphosphorylation of polycystin-2 at a critical residue in disease reveals an essential role for polycystin-1-regulated dephosphorylation. Hum. Mol. Genet. *22*, 1924–1939.
83. Sun, L., Hu, C., and Zhang, X. (2019). Histone Deacetylase Inhibitors Reduce Cysts by Activating Autophagy in Polycystic Kidney Disease. Kidney Dis. *5*, 163–172.
84. Taskén, K., and Aandahl, E.M. (2004). Localized effects of cAMP mediated by distinct routes of protein kinase A. Physiol. Rev. *84*, 137–167.

85. Tian, X., Liu, Z., Niu, B., Zhang, J., Tan, T.K., Lee, S.R., Zhao, Y., Harris, D.C.H., and Zheng, G. (2011). E-Cadherin/β-Catenin Complex and the Epithelial Barrier. J. Biomed. Biotechnol. *2011*.

86. Tunquist, B.J., Hoshi, N., Guire, E.S., Zhang, F., Mullendorff, K., Langeberg, L.K., Raber, J., and Scott, J.D. (2008). Loss of AKAP150 perturbs distinct neuronal processes in mice. Proc. Natl. Acad. Sci. *105*, 12557–12562.

87. Wallace, D.P. (2011). Cyclic AMP-mediated cyst expansion. Biochim. Biophys. Acta *1812*, 1291–1300.

88. Weber, E.J., Chapron, A., Chapron, B.D., Voellinger, J.L., Lidberg, K.A., Yeung, C.K., Wang, Z., Yamaura, Y., Hailey, D.W., Neumann, T., et al. (2016). Development of a microphysiological model of human kidney proximal tubule function. Kidney Int. *90*, 627–637.

89. Wheway, G., Nazlamova, L., and Hancock, J.T. (2018). Signaling through the Primary Cilium. Front. Cell Dev. Biol. *6*.

90. Whiting, J.L., Nygren, P.J., Tunquist, B.J., Langeberg, L.K., Seternes, O.-M., and Scott, J.D. (2015). Protein Kinase A Opposes the Phosphorylation-dependent Recruitment of Glycogen Synthase Kinase 3β to A-kinase Anchoring Protein 220. J. Biol. Chem. *290*, 19445–19457.

91. Whiting, J.L., Ogier, L., Forbush, K.A., Bucko, P., Gopalan, J., Seternes, O.-M., Langeberg, L.K., and Scott, J.D. (2016). AKAP220 manages apical actin networks that coordinate aquaporin-2 location and renal water reabsorption. Proc. Natl. Acad. Sci. *113*, E4328–E4337.

92. Wilson, P.D. (2004). Polycystic kidney disease. N. Engl. J. Med. *350*, 151–164.

93. Winyard, P., and Jenkins, D. (2011). Putative roles of cilia in polycystic kidney disease. Biochim. Biophys. Acta BBA - Mol. Basis Dis. *1812*, 1256–1262.

94. Wozniak, M.A., Modzelewska, K., Kwong, L., and Keely, P.J. (2004). Focal adhesion regulation of cell behavior. Biochim. Biophys. Acta BBA - Mol. Cell Res. *1692*, 103–119.

95. Ye, H., Wang, X., Constans, M.M., Sussman, C.R., Chebib, F.T., Irazabal, M.V., Young, W.F., Harris, P.C., Kirschner, L.S., and Torres, V.E. (2017). The regulatory 1α subunit of protein kinase A modulates renal cystogenesis. Am. J. Physiol. - Ren. Physiol. *313*, F677–F686.

96. Yui, S., Nakamura, T., Sato, T., Nemoto, Y., Mizutani, T., Zheng, X., Ichinose, S., Nagaishi, T., Okamoto, R., Tsuchiya, K., et al. (2012). Functional engraftment of colon epithelium expanded in vitro from a single adult Lgr5 + stem cell. Nat. Med. *18*, 618–623.